Magazine of Civil Engineering

ISSN 2712-8172

journal homepage: http://engstroy.spbstu.ru/

DOI: 10.18720/MCE.100.2

Free vibration of axially loaded multi-cracked Timoshenko beams

Y.S. Al Rjoub*[a], A.G. Hamad[b]

[a] *Civil Engineering Department, Jordan University of Science and Technology, Irbid, Jordan*

[b] *Jordan University of Science and Technology, Irbid, Jordan*

** E-mail: ysalrjoub@just.edu.jo*

Keywords: cracked Timoshenko beam, shear deformation, rotary inertia, free vibration, buckling load, transfer matrix.

Abstract. In this paper, the free vibration of axially-loaded, multi-cracked Timoshenko beams with differing boundary conditions, namely, hinged-hinged, fixed-fixed, fixed-hinged, and fixed-free is studied. The cracked beam system is represented as several beam segments connected by massless rotational springs with sectional flexibility. Each segment is assumed to obey the Timoshenko beam theory. A simple transfer matrix method is used to derive the characteristic equation of the axially-loaded, multi-cracked beam with differing boundary conditions. The characteristic equation and corresponding mode shapes are a function of natural frequency, crack size and location, and physical parameters of the beam. In this paper, the effects of crack depth, number of cracks, position of cracks, axial load, shear deformation and rotary inertia on the dynamic behavior of multi-cracked beams are studied in detail. It is found that there is good agreement between the results obtained in this study and results available in the literature. Additionally, interesting observations overlooked by other researchers are obtained.

1. Introduction

Many engineering structures suffer from mechanical vibrations, environmental effects, corrosion, extended service and cyclic loading, etc. that create structural defects, including cracks. These cracks change the dynamic properties of the structure, such as natural frequency and mode shape. A crack in a beam element introduces local flexibility due to strain energy concentrations in the vicinity of the crack tip under load. This flexibility changes the dynamic behavior of the structural member.

There has been much experimental and analytical research performed on the effects of cracking and damage on the safety of structures [1–5]. In this paper, the local flexibility method is used, which considers the cracked beam as several beam segments with the same properties connected by massless rotational springs. Local flexibility is used by [6] to estimate the crack stress intensity factor. The authors of [7–9] used Castigliano's theorem and fracture mechanics to compute the flexibility of the cracked region of a uniform beam with a transverse surface crack, which is a function of the ratio of crack depth to the height of the cross-section. The function was obtained experimentally, according to the measurements provided by [10]. This factor can also be obtained from [11]. Many researchers studied the free vibration of cracked Euler-Bernoulli and Timoshenko beams, both analytically and experimentally, [12–19]. The free vibration of cracked Timoshenko beams with various boundary conditions is studied by [20] using ultraspherical polynomials. The authors of [21] analyzed the free vibration of Euler-Bernoulli and Timoshenko beams resting on Pasternak and generalized elastic foundations. The free and forced vibration of cracked beams is investigated by [22–24]. Other researchers have studied the free vibration of cracked, functionally-graded Euler-Bernoulli and Timoshenko beams [25–29]. A dynamic stiffness method is used by the authors of [30] to study the free and forced vibration of multi-cracked, continuous, functionally-graded beams. An analytical solution of the forced vibration of cracked Timoshenko beams with damping is obtained by [31]. The free vibration of functionally-graded cracked Timoshenko beams is studied by [32–33]. A differential quadrature method is used by [34] to study the free and forced vibration of multi-cracked Timoshenko beams carrying a moving mass. A method is proposed by [35] which is based on the measurements of natural frequencies to detect a single crack in functionally-graded Timoshenko beam. In this paper, the transfer matrix method (TMM) is used

to study the free vibration of axially-loaded, cracked beams. This method was first introduced by [36], and used by other researchers [37–41] to study the free vibration of cracked beams. Other researchers solved the problem using the finite element method, [42–44].

According to the authors' knowledge, the effects of four cracks on the dynamic behavior of axially-loaded Timoshenko beams have not been studied in detail in the existing literature. In this paper, the dynamic behavior of a multi-cracked beam under axial loading including the shear deformation and rotary inertia and their coupling effects with differing boundary conditions with an arbitrary number of transverse cracks is investigated. The simple transfer matrix method is used to ascertain the natural frequencies and corresponding mode shapes of the beam. Some results obtained in this paper are compared to those results available in literature.

2. Methods

2.1. Theoretical model

Consider a multi-cracked beam with length l, cross-sectional area of width b and height h, and a number of single-sided, open cracks located at points x_{c1}, x_{c2}, …, x_{ci} with sizes $a_{c,1}$, $a_{c,2}$, …, $a_{c,i}$, respectively, as shown in Fig. 1.

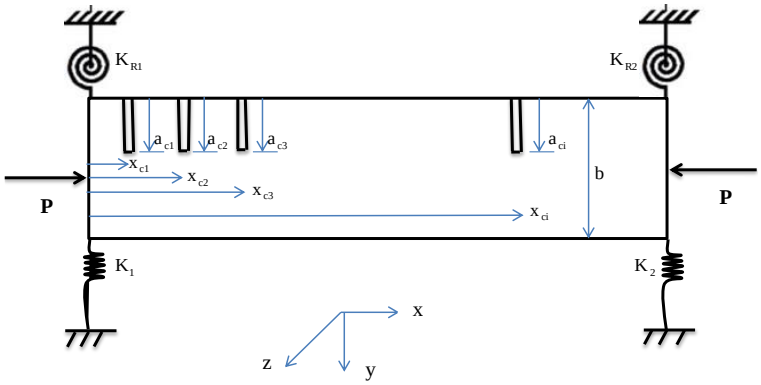

Figure 1. A multi-cracked, axially loaded beam with *i* edge open cracks, restrained by linear and rotational springs at both ends.

The boundary conditions are represented with linear and rotational springs at both ends (K_1, K_{R1}, K_2, and K_{R2}). Timoshenko (1921) proposed a beam theory which adds the effects of shear and rotation to the governing equation of motion of an Euler- Bernoulli beam. The total slope $\frac{\partial y(x,t)}{\partial x}$ is a combination of the bending slope $\psi(x,t)$ and the shear slope $\gamma_{xy}(x,\mathrm{t})$ [46], which can be written as:

$$\frac{\partial y(x,t)}{\partial x} = \psi(x,t) + \gamma_{xy}(x,t) \tag{1}$$

where $\psi(x,t)$, $\gamma_{xy}(x,\mathrm{t})$,and t are the bending slope, the shear slope, and the time parameter, respectively.

In [47], it was assumed that the component of axial load P on the cross section is acting on the plane of the total slope. Accordingly, the shear force can be written as:

$$V(x,t) + P\frac{\partial y(x,t)}{\partial x} = \left[\frac{\partial y(x,t)}{\partial x} - \psi(x,t)\right]k' \tag{2}$$

where V is the shear force (along the *y*-axis), A is the area of beam cross section, G is the shear modulus and k' is the shear correction factor (assumed equal to 5/6 in this paper). The dynamic equilibrium equations for the free-body diagram shown in Fig. 2.b becomes:

$$-V(x,t) + \frac{\partial M(x,t)}{\partial x} - P\frac{\partial y(x,t)}{\partial x} + \rho I\frac{\partial^2 \psi}{\partial t^2} = 0 \tag{3}$$

And,

$$\frac{\partial V(x,t)}{\partial x} = \frac{\partial^2 y(x,t)}{\partial t^2} \tag{4}$$

where M is the bending moment (about the *z*-axis), ρ is the material density, and I is the moment of inertia. Using Eqns. (3) and (4), one can obtain the governing equation for the transverse vibration of a uniform Timoshenko beam subjected to constant axial force as:

$$EI\left(\frac{k'GA-P}{k'GA}\right)\frac{\partial^4 y(x,t)}{\partial x^4} + m + P\frac{\partial^2 y(x,t)}{\partial x^2} - mr^2\left(\frac{k'GA-P}{k'GA}\right)\frac{\partial^4 y(x,t)}{\partial x^2 \partial t^2} - \frac{mEI}{k'GA}\frac{\partial^4 y(x,t)}{\partial x^2 \partial t^2} + \frac{m^2 r^2}{k'GA}\frac{\partial^4 y(x,t)}{\partial t^4} = 0 \tag{5a}$$

In a similar manner, Eqn. (5a) can be written in terms of the deflection slope alone as:

$$EI\left(\frac{k'GA-P}{k'GA}\right)\frac{\partial^4 \psi(x,t)}{\partial x^4} + m + P\frac{\partial^2 \psi(x,t)}{\partial x^2} - mr^2\left(\frac{k'GA-P}{k'GA}\right)\frac{\partial^4 \psi(x,t)}{\partial x^2 \partial t^2} - \frac{mEI}{k'GA}\frac{\partial^4 \psi(x,t)}{\partial x^2 \partial t^2} + \frac{m^2 r^2}{k'GA}\frac{\partial^4 \psi(x,t)}{\partial t^4} = 0 \tag{5b}$$

where *m* is the mass per unit length, *r* is the radius of gyration; $K'A$ is the effective shear area of the cross section.

It is clear that Eqn. (5a) reduces to Euler beam theory (EBT) when the shear deformation and rotary inertia are equal to zero. Then Eqn. (5a) become:

$$EI\frac{\partial^4 (y,t)}{\partial x^4} + m\frac{\partial^2 (y,t)}{\partial x^2} + P\frac{\partial^2 (y,t)}{\partial x^2} = 0$$

A simple transfer matrix method is used to get the general form of the characteristic equation for the axially-loaded cracked beam, which is a function of frequency, axial load, the locations and sizes of the cracks, boundary conditions, and the geometrical and physical parameters of the beam. It is assumed that a beam with n segments is joined by massless, rotational springs, as shown in Fig. 2.

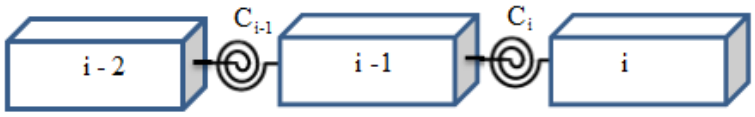

Figure 2. Beam elements joined by massless, rotational spring.

The free vibration solution for a Timoshenko beam (TBT) subjected to axial load can be found using the method of separation of variables as:

$$y(x,t) = Y(x)e^{i\omega t} \tag{6a}$$

$$\psi(x,t) = \psi(x)e^{i\omega t} \tag{6b}$$

where, $Y(x)$, $\psi(x)$, ω, i, and x are the normal function of $y(x,t)$, the normal function of $\psi(x,t)$, the circular frequency, the imaginary number, and the spatial position on the *x*-axis, respectively.

Substituting Eqn. (6a) into Eqn. (5a) leads to:

$$EI\left(\frac{k'GA-P}{k'GA}\right)\frac{\partial^4 Y(x)}{\partial x^4}+m\omega^2 Y(x)+P\frac{\partial^2 Y(x)}{\partial x^2}- mr^2\omega^2\left(\frac{k'GA-P}{k'GA}\right)\frac{\partial^2 Y(x)}{\partial x^2}-\frac{mEI\omega^2}{k'GA}\frac{\partial^2 Y(x)}{\partial x^2}+\frac{m^2r^2\omega^4}{k'GA}Y(x)=0 \quad (7a)$$

And, substituting Eqn. (6b) into Eqn. (5b) yields:

$$EI\left(\frac{k'GA-P}{k'GA}\right)\frac{\partial^4 \psi(x)}{\partial x^4}+m\omega^2+P\frac{\partial^2 \psi(x)}{\partial x^2}- mr^2\omega^2\left(\frac{k'GA-P}{k'GA}\right)\frac{\partial^2 \psi(x)}{\partial x^2}-\frac{mEI\omega^2}{k'GA}\frac{\partial^2 \psi(x)}{\partial x^2}+\frac{m^2r^2\omega^4}{k'GA}\psi(x)=0 \quad (7b)$$

The general-form solutions of Eqn. (7a) and (7b) are:

$$Y(x)=A_1\cos(\alpha x)+A_2\sin(\alpha x)+A_3\cosh(\beta x)+A_4\sinh(\beta x) \quad (8a)$$

$$\psi(x)=m_1A_1\cos(\alpha x)+m_1A_2\sin(\alpha x)+m_2A_3\cosh(\beta x)+m_2A_4\sinh(\beta x) \quad (8b)$$

where,

$$\alpha=\sqrt{\frac{1}{2}\left(\frac{mr^2\omega^2}{EI}+\frac{m\omega^2}{k'AG\zeta}+\frac{P}{EI\xi}\right)^2+\frac{1}{2}\sqrt{\left(\frac{mr^2\omega^2}{EI}+\frac{m\omega^2}{k'AG\zeta}+\frac{P}{EI\xi}\right)^2-4\left(\frac{mr^2\omega^2}{EIk'GA\xi}-\frac{m\omega^2}{EI\xi}\right)}},$$

$$\beta=\sqrt{-\frac{1}{2}\left(\frac{mr^2\omega^2}{EI}+\frac{m\omega^2}{k'AG\zeta}+\frac{P}{EI\xi}\right)^2+\frac{1}{2}\sqrt{\left(\frac{mr^2\omega^2}{EI}+\frac{m\omega^2}{k'AG\zeta}+\frac{P}{EI\xi}\right)^2-4\left(\frac{mr^2\omega^2}{EIk'GA\xi}-\frac{m\omega^2}{EI\xi}\right)}},$$

where $\xi=\frac{k'GA-P}{k'GA}$, $\mathrm{m}_1=\frac{\rho A\omega^2}{k'GA\alpha}-\alpha$, $\mathrm{m}_2=\frac{\rho A\omega^2}{k'GA\beta}+\beta$ and A_1 to A_4 are unknown constants.

The slope $\theta(x)$, bending moment $M(x)$, and shear force $V(x)$ can be obtained as:

$$\theta(x)=\frac{\partial Y(x)}{\partial x}=m_1\left[-A_1\sin(\alpha x)+A_2\cos(\alpha x)\right]+m_2\left[-A_3\sinh(\beta x)-A_4\cosh(\beta x)\right] \quad (9a)$$

$$M(x)=n_1\left[-A_1\cos(\alpha x)-A_2\sin(\alpha x)\right]+n_2\left[A_3\cosh(\beta x)+A_4\sinh(\beta x)\right] \quad (9b)$$

$$V(x)=b_1\left[A_1\sin(\alpha x)-A_2\cos(\alpha x)\right]+b_2\left[A_3\sinh(\beta x)+A_4\cosh(\beta x)\right] \quad (9c)$$

where $n_1=E\,\mathrm{Im}_1\,\alpha$, $n_2=-E\,\mathrm{Im}_2\,\beta$, $b_1=E\,\mathrm{Im}_1\,\alpha^2-m_1\rho I\omega^2$, $b_2=-E\,\mathrm{Im}_2\,\alpha^2-m_2\rho I\omega^2$.

The $[S(x)]$ matrix can be obtained from Eqn. (8a) and (9a-c) as:

$$[S(x)]=\begin{bmatrix} \cos(\alpha x) & \sin(\alpha x) & \cosh(\beta x) & \sinh(\beta x) \\ -m_1\sin(\alpha x) & m_1\cos(\alpha x) & -m_2\sinh(\beta x) & -m_2\cosh(\beta x) \\ -n_1\cos(\alpha x) & -n_1\sin(\alpha x) & n_2\cosh(\beta x) & n_2\sinh(\beta x) \\ b_1\sin(\alpha x) & -b_1\cos(\alpha x) & b_2\sinh(\beta x) & b_2\cosh(\beta x) \end{bmatrix} \quad (10)$$

The compatibility requirements at the crack position, x_c, which are the continuity of the deflection, bending moment, shear force, and the discontinuity of slopes for segments i and i+1, can be written in matrix form as:

$$\begin{Bmatrix} Y_{i+1}(x_c) \\ \theta_{i+1}(x_c) \\ M_{i+1}(x_c) \\ V_{i+1}(x_c) \end{Bmatrix} = \begin{bmatrix} 1 & 0 & 0 & 0 \\ 0 & 1 & C_i & 0 \\ 0 & 0 & 1 & 0 \\ 0 & 0 & 0 & 1 \end{bmatrix} \begin{Bmatrix} Y_i(x_c) \\ \theta_i(x_c) \\ M_i(x_c) \\ V_i(x_c) \end{Bmatrix} \quad (11)$$

where C_i is the flexibility coefficient at the i[th] crack, and depend on the load case of the cracked element.

2.2. Local flexibility due to a crack

An open crack on an elastic structure can be considered a source of local flexibility due to the strain energy concentration at the surrounding area of the crack tip. The idea of replacing a crack with a massless spring is presented to establish the relation between the strain energy concentration and applied loads. The flexibility coefficients are expressed in terms of stress intensity factors, utilizing Castigliano's theorem. Generalized loading conditions for abeam element of circular or rectangular cross section with a transverse surface crack are shown in Fig. 3.

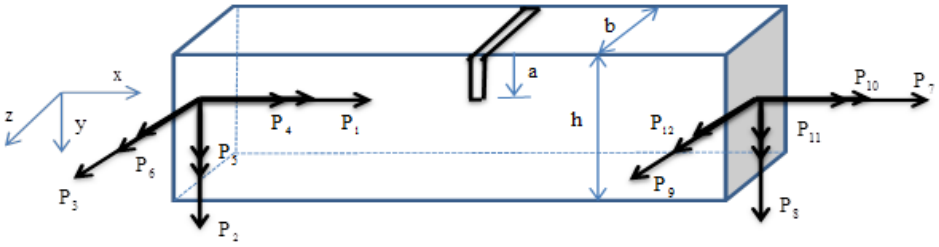

Figure 3. Model of the cracked element.

The crack has a tip line parallel to the z-axis and the bar is loaded by shear forces P_2, P_3, P_8, and P_9; bending moments P_4, P_5, P_{11}, and P_{12}; axial forces P_1 and P_7; and torsional moments P_4 and P_{10}. According to Castigliano's theorem, the additional displacement caused by the crack is given as:

$$u_i = \frac{\partial U}{\partial P_i} = \frac{\partial}{\partial P_i}\left[\int_{Ac} J dA\right] \quad (12)$$

where U, A_c, and J are the strain energy due to the crack, the crack section, and strain energy density function, respectively.

The strain energy density function can be expressed according to [14] for plane stress as: 1

$$J = \left(\frac{1-\nu^2}{E}\right)\left[\left(\sum_{i=1}^{6} K_{Ii}\right)^2 + \left(\sum_{i=1}^{6} K_{IIi}\right)^2 + (1+\nu)\left(\sum_{i=1}^{6} K_{IIIi}\right)^2\right] \quad (13)$$

where, ν is Poisson's ratio and K_{Ii}, K_{IIi}, K_{IIIi} are the crack stress intensity factors for opening mode, shearing mode, and tearing mode, respectively; I = 1,2,…,6.

Stress intensity factors can be calculated following [14] as:

$$K_{I1} = \sigma_1 \sqrt{\pi a} F_1(a/h), \sigma_1 = \frac{P_1}{bh}$$

$$K_{I5} = \sigma_5 \sqrt{\pi a} F_1(a/h), \sigma_5 = \frac{12 P_5 z}{b^3 h}$$

$$K_{I6} = \sigma_6 \sqrt{\pi a} F_2(a/h), \sigma_6 = \frac{6 P_6}{bh^2}$$

$$K_{I2} = K_{I3} = K_{I4} = 0$$

$$K_{II2} = \sigma_2 \sqrt{\pi a} F_{II}(a/h), \sigma_2 = \frac{kP_2}{bh}$$

$$K_{II4} = \sigma_4 \sqrt{\pi a} F_{II}(a/h), \sigma_4 = \frac{P_4}{bh} \quad (14)$$

$$K_{II1} = K_{II3} = K_{II5} = K_{II6} = 0$$

$$K_{III3} = \sigma_3 \sqrt{\pi a} F_{III}(a/h), \sigma_3 = \frac{kP_3}{bh}$$

$$K_{III4} = \sigma_{4III} \sqrt{\pi a} F_{III}(a/h), \sigma_{4III} = \frac{P_4}{bh}$$

$$K_{III1} = K_{III2} = K_{III5} = K_{III6} = 0$$

where

$$F_1(a/h) = \sqrt{\frac{2h}{\pi a} \tan\left(\frac{\pi a}{2h}\right)} \frac{0.752 + 2.02\left(\frac{a}{h}\right) + 0.37\left(1 - \sin\left(\frac{\pi a}{2h}\right)\right)^3}{\cos\left(\frac{\pi a}{2h}\right)}$$

$$F_2(a/h) = \sqrt{\frac{2h}{\pi a} \tan\left(\frac{\pi a}{2h}\right)} \frac{0.923 + 0.199\left(1 - \sin\left(\frac{\pi a}{2h}\right)\right)^4}{\cos\left(\frac{\pi a}{2h}\right)} \quad (15)$$

$$F_{II}(a/h) = \frac{1.122 - 0.561\left(\frac{a}{h}\right) + 0.085\left(\frac{a}{h}\right)^2 + 0.18\left(\frac{a}{h}\right)^3}{\sqrt{1 - \left(\frac{a}{h}\right)}}$$

$$F_{III}(a/h) = \sqrt{\frac{2h}{\pi a} \tan\left(\frac{\pi a}{2h}\right)}$$

From Eqns. (12), (14) and (15), the flexibility coefficients can be calculated as:

$$C_{11} = (1 - \nu^2) \frac{2\pi}{Eb^2} \left[\int_0^{\varphi} \phi F_1^2(\phi) d\phi\right] \int_{-b/2}^{b/2} dz$$

$$C_{15}=C_{51}=(1-\nu^2)\frac{24\pi}{Eb^4}[\int_0^{\varphi}\phi F_1^2(\phi)d\phi]\int_{-b/2}^{b/2}zdz$$

$$C_{16}=C_{61}=(1-\nu^2)\frac{12\pi}{Eb^2h}[\int_0^{\varphi}\phi F_1(\phi)F_2(\phi)d\phi]\int_{-b/2}^{b/2}dz$$

$$C_{22}=(1-\nu^2)\frac{2k^2\pi}{Eb^2}[\int_0^{\varphi}\phi F_{II}^2(\phi)d\phi]\int_{-b/2}^{b/2}dz$$

$$C_{24}=C_{42}=(1-\nu^2)\frac{2k\pi}{Eb^2}[\int_0^{\varphi}\phi F_{II}^2(\phi)d\phi]\int_{-b/2}^{b/2}dz$$

$$C_{33}=(1-\nu^2)\frac{2k^2\mu\pi}{Eb^2}[\int_0^{\varphi}\phi F_{III}^2(\phi)d\phi]\int_{-b/2}^{b/2}dz$$

$$C_{34}=C_{43}=(1-\nu^2)\frac{2k\mu\pi}{Eb^2}[\int_0^{\varphi}\phi F_{III}^2(\phi)d\phi]\int_{-b/2}^{b/2}dz \quad (16)$$

$$C_{44}=(1-\nu^2)\frac{2\pi}{Eb^2}[\int_0^{\varphi}\phi(F_{II}^2(\phi)+\mu F_{III}^2(\phi))d\phi]\int_{-b/2}^{b/2}dz$$

$$C_{55}=(1-\nu^2)\frac{288\pi}{Eb^6}[\int_0^{\varphi}\phi F_1^2(\phi)d\phi]\int_{-b/2}^{b/2}z^2dz$$

$$C_{56}=C_{65}=(1-\nu^2)\frac{144\pi}{Eb^4h}[\int_0^{\varphi}\phi F_1^2(\phi)F_2(\phi)d\phi]\int_{-b/2}^{b/2}zdz$$

$$C_{66}=(1-\nu^2)\frac{72\pi}{Eb^2h^2}[\int_0^{\varphi}\phi F_2^2(\phi)d\phi]\int_{-b/2}^{b/2}dz$$

where $\mu=1+\nu$, $\phi=\frac{a}{h}$ and k is a shape coefficient for a rectangular cross section.

In this study, the flexural vibration of the beam is the only significant load in the equations above. Therefore, the contribution of the axial load component to the strain energy of the system is very small. Hence, the only component in the flexibility matrix is C_{66}.

2.3. Transfer matrix method

Equation (11) can be written as:

$$\{Q_{i+1}(x_i)\}=[C_i]\{Q_i(x_i)\} \quad (17)$$

At the location of open edge crack, the two beam segments i and i+1 are connected by a massless, rotational springs, as shown in Fig. 2. Equation (6a) and Eqn. (8a) and Eqns. (9a) to (9c) can be written in matrix form for both segments i, and i+1, respectively, as:

$$\begin{Bmatrix} Y_i(x) \\ \theta_i(x) \\ M_i(x) \\ V_i(x) \end{Bmatrix} = [S(x)] \begin{Bmatrix} A_{1,i} \\ A_{2,i} \\ A_{3,i} \\ A_{4,i} \end{Bmatrix} \tag{18a}$$

$$\begin{Bmatrix} Y_{i+1}(x) \\ \theta_{i+1}(x) \\ M_{i+1}(x) \\ V_{i+1}(x) \end{Bmatrix} = [S(x)] \begin{Bmatrix} A_{1,i+1} \\ A_{2,i+1} \\ A_{3,i+1} \\ A_{4,i+1} \end{Bmatrix} \tag{18b}$$

Equation (18a) can be rewritten for a segment, $x_{i-1} < x < x_i$, as:

$$\{Q_i(x)\} = [S(x)]\{A_i\} \tag{19}$$

where,

$$\{Q_i(x)\} = \begin{Bmatrix} Y_{i+1}(x_c) \\ \theta_{i+1}(x_c) \\ M_{i+1}(x_c) \\ V_{i+1}(x_c) \end{Bmatrix}, \text{ and } \{A_i\} = \begin{Bmatrix} A_{1,i} \\ A_{2,i} \\ A_{3,i} \\ A_{4,i} \end{Bmatrix}$$

The boundary conditions of the beam using equilibrium equations can be expressed as:

$$M(0) = K_{R1}\theta(0) \tag{20a}$$

$$V(0) = -K_1 Y(0) \tag{20b}$$

$$M(l) = -K_{R2}\theta(l) \tag{20c}$$

$$V(l) = K_2 Y(l) \tag{20d}$$

In order to calculate the natural frequencies and corresponding mode shapes, the characteristic equation can be derived as in [48].

The continuity conditions of the deflection, slope, moment, and shear at $x = 0$ and $\mathrm{x} = l$ leads to:

$$\begin{Bmatrix} Y_{i+1}(l) \\ \theta_{i+1}(l) \\ -K_{R2}\theta_{i+1}(l) \\ K_2 Y_{i+1}(l) \end{Bmatrix} = [T] \begin{Bmatrix} Y_1(0) \\ \theta_1(0) \\ K_{R1}\theta_1(0) \\ -K_1 Y_1(0) \end{Bmatrix} \tag{21}$$

where $[T] = \begin{bmatrix} T_{11} & T_{12} & T_{13} & T_{14} \\ T_{21} & T_{22} & T_{23} & T_{24} \\ T_{31} & T_{32} & T_{33} & T_{34} \\ T_{41} & T_{42} & T_{43} & T_{44} \end{bmatrix}$

Rewriting equation (21) as:

$$\begin{Bmatrix} Y_{i+1}(l) \\ \theta_{i+1}(l) \end{Bmatrix} = \begin{bmatrix} T_{11} - K_1 T_{14} & T_{12} + K_{R1} T_{13} \\ T_{21} - K_1 T_{24} & T_{22} + K_{R1} T_{23} \end{bmatrix} \begin{Bmatrix} Y_1(0) \\ \theta_1(0) \end{Bmatrix} \tag{22a}$$

$$\begin{Bmatrix} -K_{R2}\theta_{i+1}(l) \\ K_2 Y_{i+1}(l) \end{Bmatrix} = \begin{bmatrix} T_{31} - K_1 T_{34} & T_{32} + K_{R1} T_{33} \\ T_{41} - K_1 T_{44} & T_{42} + K_{R1} T_{43} \end{bmatrix} \begin{Bmatrix} Y_1(0) \\ \theta_1(0) \end{Bmatrix} \quad (22b)$$

The characteristic equation can be obtained by substitution of Equation (22a) into Equation (22b).

$$F_1 F_4 - F_2 F_3 = 0 \quad (23)$$

where,

$$F_1 = -K_{R2} T_{21} + K_1 K_{R2} T_{24} - T_{31} + K_1 T_{34}$$

$$F_2 = -K_{R2} T_{22} - K_{R1} K_{R2} T_{23} - T_{32} - K_{R1} T_{33}$$

$$F_3 = K_2 T_{11} - K_1 K_2 T_{14} - T_{41} + K_1 T_{44}$$

$$F_4 = K_2 T_{12} + K_2 K_{R1} T_{13} - T_{42} - K_{R1} T_{43}$$

Characteristic Eqn. (23) can be derived for different boundary conditions as:

a. For fixed-free boundaries $\left(K_1 = K_{R1} = \infty\right)$,

$$T_{34} T_{43} - T_{33} T_{44} = 0$$

b. For pinned-pinned boundaries $\left(K_1 = K_2 = \infty\right)$,

$$T_{34} T_{12} - T_{32} T_{14} = 0$$

c. For fixed-pinned boundaries, $\left(K_1 = K_2 = K_{R1} = \infty\right)$,

$$T_{34} T_{13} - T_{33} T_{14} = 0$$

d. For fixed-fixed boundaries, $\left(K_1 = K_2 = K_{R1} = K_{R_2} = \infty\right)$,

$$T_{24} T_{13} - T_{23} T_{14} = 0$$

e. For free-free boundaries,

$$T_{31} T_{42} - T_{32} T_{41} = 0$$

2.4. The corresponding mode shapes

In order to obtain the mode shape of the axially-loaded, cracked Euler beam, the unknown constants $\{A_i\}$ for each sub-segment of the cracked beam can be determined. At first, the unknown coefficients for the first segment, $\{A_1\}$, are determined. Then, the unknown coefficients for the other segments may be obtained, using the following procedure.

1. At x = 0, Eqn. (19) can be written as:

$$\begin{Bmatrix} Y_1(0) \\ \theta_1(0) \\ K_{R1}\theta_1(0) \\ -K_1 Y_1(0) \end{Bmatrix} = \begin{bmatrix} 1 & 0 & 1 & 0 \\ 0 & \alpha & 0 & \beta \\ -EI\alpha^2 & 0 & EI\beta^2 & 0 \\ 0 & -(EI\alpha^3 - P_\alpha) & 0 & (EI\beta^3 + P\beta \end{bmatrix} \begin{Bmatrix} A_{1,1} \\ A_{2,1} \\ A_{3,1} \\ A_{4,1} \end{Bmatrix} \quad (24)$$

Eqn. (24) can be rewritten as:

$$\begin{Bmatrix} Y_1(0) \\ \theta_1(0) \end{Bmatrix} = \begin{bmatrix} 1 & 0 & 1 & 0 \\ 0 & \alpha & 0 & \beta \end{bmatrix} \begin{Bmatrix} A_{1,1} \\ A_{2,1} \\ A_{3,1} \\ A_{4,1} \end{Bmatrix} \tag{25a}$$

$$\begin{Bmatrix} -K_1\theta_1(0) \\ K_{R1}Y_1(0) \end{Bmatrix} = \begin{bmatrix} -EI\alpha^2 & 0 & EI\beta^2 & 0 \\ 0 & -(EI\alpha^3 - P\alpha) & 0 & (EI\beta^3 + P\beta) \end{bmatrix} \begin{Bmatrix} A_{1,1} \\ A_{2,1} \\ A_{3,1} \\ A_{4,1} \end{Bmatrix} \tag{25b}$$

Substituting Eqn. (25a) into Eqn. (25b) yields:

$$\begin{bmatrix} Q_{11} & Q_{12} & Q_{13} & Q_{14} \\ Q_{21} & Q_{22} & Q_{23} & Q_{24} \end{bmatrix} \begin{Bmatrix} A_{1,1} \\ A_{2,1} \\ A_{3,1} \\ A_{4,1} \end{Bmatrix} = 0 \tag{26}$$

where,

$$\begin{gathered} Q_{11} = n_1,\ Q_{12} = K_{R1}m_1,\ Q_{13} = -n_2,\ Q_{14} = -K_{R1}m_2, \\ Q_{21} = -K_1\ Q_{22} = b_1,\ Q_{23} = -K_1,\ Q_{24} = -b_2 \end{gathered} \tag{27}$$

2. At $x = l$, substituting Eqns. (10), (20c), (20d), and (19) into Eqn. (21) yields:

$$\begin{Bmatrix} Y_{i+1}(l) \\ \theta_{i+1}(l) \end{Bmatrix} = \begin{bmatrix} T_{11} - EI\alpha^2 T_{13} & (T_{12}\alpha - T_{14}(EI\alpha^3 - P\alpha)) & T_{11} + EIT_{13}\beta^2 & (T_{12}\beta + T_{14}(EI\beta^3 + P\beta)) \\ T_{21} - EIT_{23}\alpha^2 & (T_{22}\alpha - T_{24}(EI\alpha^3 - P\alpha)) & T_{21} + EIT_{23}\beta^2 & (T_{22}\beta + T_{24}(EI\beta^3 + P\beta)) \end{bmatrix} \begin{Bmatrix} A_{1,1} \\ A_{2,1} \\ A_{3,1} \\ A_{4,1} \end{Bmatrix} \tag{28a}$$

$$\begin{Bmatrix} -K_{R2}\theta_{i+1}(l) \\ K_2 Y_{i+1}(l) \end{Bmatrix} = \begin{bmatrix} T_{31} - EI\alpha^2 T_{33} & (T_{32}\alpha - T_{34}(EI\alpha^3 - P\alpha)) & T_{31} + EIT_{33}\beta^2 & (T_{32}\beta + T_{34}(EI\beta^3 + P\beta)) \\ T_{41} - EIT_{43}\alpha^2 & (T_{42}\alpha - T_{44}(EI\alpha^3 - P\alpha)) & T_{41} + EIT_{43}\beta^2 & (T_{42}\beta + T_{44}(EI\beta^3 + P\beta)) \end{bmatrix} \begin{Bmatrix} A_{1,1} \\ A_{2,1} \\ A_{3,1} \\ A_{4,1} \end{Bmatrix} \tag{28b}$$

Substituting Eqn. (38a) into Eqn. (38b) leads to:

$$\begin{bmatrix} Q_{31} & Q_{32} & Q_{33} & Q_{34} \\ Q_{41} & Q_{42} & Q_{43} & Q_{44} \end{bmatrix} \begin{Bmatrix} A_{1,1} \\ A_{2,1} \\ A_{3,1} \\ A_{4,1} \end{Bmatrix} = 0 \tag{29}$$

where,

$$\begin{gathered} Q_{31} = -K_{R2}(T_{21} - n_1T_{23}) - T_{31} + n_1T_{33} \\ Q_{32} = -K_{R2}(m_1T_{22} - b_1T_{24}) - (m_1T_{32} - b_1T_{34}) \\ Q_{33} = -K_{R2}(T_{21} + n_2T_{23}) - T_{31} - n_2T_{33} \\ Q_{34} = -K_{R2}(-m_2T_{22} + b_2T_{24}) - (-m_2T_{32} + b_2T_{34}) \\ Q_{41} = K_2(T_{11} - n_1T_{13}) - T_{41} + n_1T_{43} \\ Q_{42} = K_2(m_1T_{12} - b_1T_{14}) - (m_1T_{42} - b_1T_4) \\ Q_{43} = K_2(T_{11} + n_2T_{13}) - T_{41} - n_2T_{43} \\ Q_{44} = K_2(-m_2T_{12} + b_2T_{14}) - (-m_2T_{42} + b_2T_{44}) \end{gathered} \tag{30}$$

Combining Eqn. (26) and Eqn. (29) yields:

$$\begin{bmatrix} Q_{11} & Q_{12} & Q_{13} & Q_{14} \\ Q_{21} & Q_{22} & Q_{23} & Q_{24} \\ Q_{31} & Q_{32} & Q_{33} & Q_{34} \\ Q_{41} & Q_{42} & Q_{43} & Q_{44} \end{bmatrix} \begin{Bmatrix} A_{1,1} \\ A_{2,1} \\ A_{3,1} \\ A_{4,1} \end{Bmatrix} = 0 \tag{31}$$

The unknown coefficients of Eqn. (31) correspond to the mode shapes of the first crack position, i.e. at $x = x_{c1}$. For other crack locations, the unknown coefficients can be obtained using the coefficients of the previous crack as:

$$\{A_i\} = [S(x_{i-1})]^{-1}[C_{i-1}][S(x_{i-1})]\{A_{i-1}\} \tag{32}$$

3. Results and Discussion

3.1. Validation of results

The present results obtained are compared with those found by [45]. Three different boundary conditions are used, namely, hinged-hinged, fixed-hinged, and fixed-fixed. Also, two different values of P/P_{cr} are used, which are 0.2 and -0.2. P_{cr} is the critical buckling load of the intact beam and it is equal to $\frac{P_E}{1+\frac{P_E}{k`GA}}$, where P_E is the Euler buckling load. Values of l = 1 m, b = 0.1 m, h = 0.2 m, E = 200 GPa, $\rho = 7850 kg/m^3$, and $\nu = 0.3$ are used as the geometrical and material properties of the intact beam. Fig. 4 a-c show the first non-dimensional natural frequency ratio $\omega_{cr} / \omega_{in}$ obtained in this study versus the non-dimensional crack location x/l for a beam with a/h = 0.1, a/h = 0.3, and a/h = 0.5, for hinged-hinged, fixed-hinged, and fixed-fixed beams, respectively, compared with those obtained by [45]. As you can see, the obtained results agree well with those reported by [45].

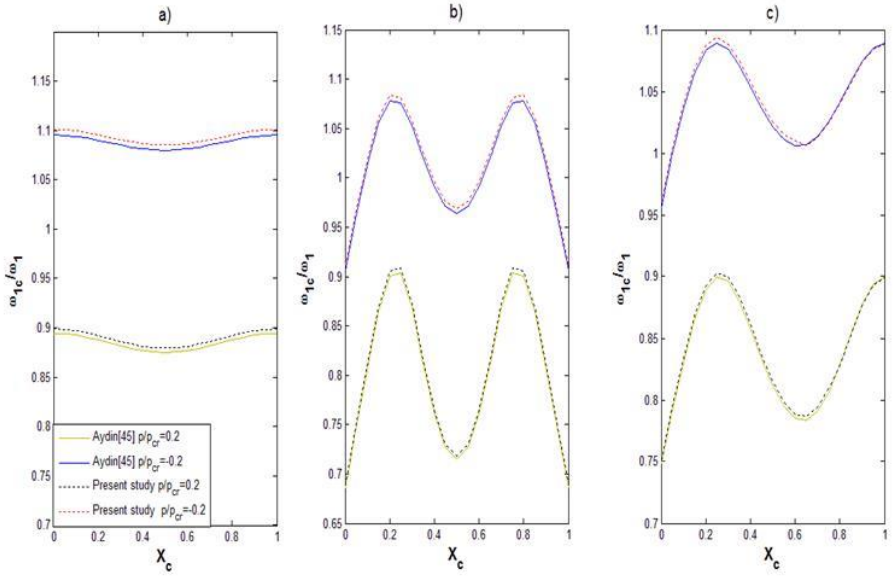

Figure 4. The first non-dimensional natural frequencies of a) hinged-hinged beam with single crack with a/h = 0.1, b) fixed-fixed beam with single crack with a/h = 0.3, and c) fixed-hinged beam with single crack with a/h = 0.5. The curves are obtained for P / P_{cr} values of -0.2, and 0.2 (from top to bottom).

3.2. Effects of One Crack and Axial Load on Natural Frequencies

In all subsequent sections, the geometrical and material properties of the intact beam are the same as those used in validation section, unless otherwise noted. The first three non-dimensional natural frequencies of a beam with a single crack versus crack location, for hinged-hinged, fixed-fixed, fixed-hinged, and fixed-free

boundary conditions, respectively, are shown in Fig. 5, 6, 7, and 8. In all figures, figure a) represents P/P_{cr} = 0, figure b) represents P/P_{cr} = -0.3, and figure c) represents P/P_{cr} = 0.3. Also, in all figures, eight values of aspect ratio a/h are used, 0, 0.1, 0.2, 0.3, 0.4, 0.5, 0.6, and 0.7. It is clear that the natural frequencies do not change with differing values of aspect ratio (a/h) at the location of zero-crossing of the mode shape and at critical points for a given frequency but do vary with differing boundary conditions. As an example, the zero-crossing points for hinged-hinged boundary conditions are located at 0.*33l*, and 0.66*l* for the third, non-dimensional natural frequency. The critical points are located at 0.11*l* and 0.89*l* for fixed-fixed boundary conditions and at 0.12*l* for fixed-hinged boundary conditions for the second, non-dimensional natural frequency. An interesting observation overlooked by researchers is that the locations of critical points for the first non-dimensional frequencies are shifted toward the center of the beam when the beam is axially loaded in compression and toward the fixed supports of the beam when the beam is axially loaded in tension for fixed-fixed and fixed-hinged boundaries. Those locations are at 0.23*l*, 0.77*l*, and at 0.21*l*, 0.79*l*, for compression- and tension-loaded beams, respectively, for fixed-fixed boundaries, and 0.27*l* and 0.25*l* for tension- and compression-loaded beams, respectively, for fixed-hinged boundaries. As most researchers have found, the beam's natural frequencies are independent of crack location. Also, the natural frequency decreases with increasing aspect ratio. The first non-dimensional frequencies are most affected by the severity of cracks and the magnitude of the axial force. For axially loaded beams, since the compressive force softens the beam and tensile force stiffens the beam, the non-dimensional natural frequencies for all modes of the beam under compressive force are smaller than those of the same beam under tensile load for all boundary conditions. The first non-dimensional natural frequency shows a maximum 14 % and 20 % increase when the cracks are located near the supports and 16 % and 29 % decrease when the cracks are located at mid-span of the beam for P/P_{cr} = 0.3 and P/P_{cr} = -0.3, respectively, for an aspect ratio of 0.5, for an axially-loaded, hinged-hinged beam. for axially-loaded fixed-fixed beams, the first non-dimensional natural frequency shows a maximum 12 % increase when the cracks are located near the supports and 15 % decrease when the cracks are located at mid-span of the beam for P/P_{cr} = -0.3 and P/P_{cr} = 0.3 respectively, for aspect ratio of 0.1, and a maximum 15 % increase and 19 % decrease for P/P_{cr} = -0.3 and P/P_{cr} = 0.3 respectively, for an aspect ratio of 0.5. The values of percent increase or decrease are increased as the value of aspect ratio increases. For axially-loaded, fixed-hinged beam, the first non-dimensional natural frequency shows a maximum 13 % increase and 16 % decrease for P/P_{cr} =-0.3 and P/P_{cr} = 0.3 respectively, for an aspect ratio of 0.1, and a maximum 16 % increase and 20 % decrease for P/P_{cr} = -0.3 and P/P_{cr} = 0.3 respectively, for an aspect ratio of 0.6. Again, for axially-loaded fixed-free beam, the first non-dimensional natural frequency shows a maximum 15 % decrease and 13% increase for P/P_{cr} =-0.3 and P/P_{cr} = 0.3 respectively, for an aspect ratio of 0.1. A maximum 24 % decrease and 16% increase are obtained for P/P_{cr} = -0.3 and P/P_{cr} = 0.3 respectively, for an aspect ratio of 0.5. Another interesting point overlooked by researchers that for fixed-free beam, the first non-dimensional natural frequencies is not affected by crack location, aspect ratio of the crack, or the magnitude of axial load beyond 0.86*l*, 0.8*l*, and 0.92*l* of the beam for zero axial load, tensile load and compressive load, respectively compressive load, respectively.

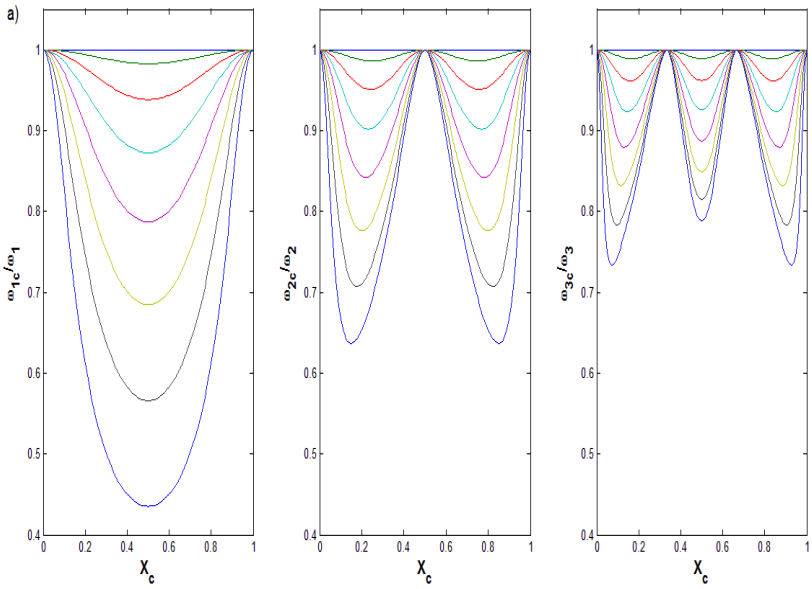

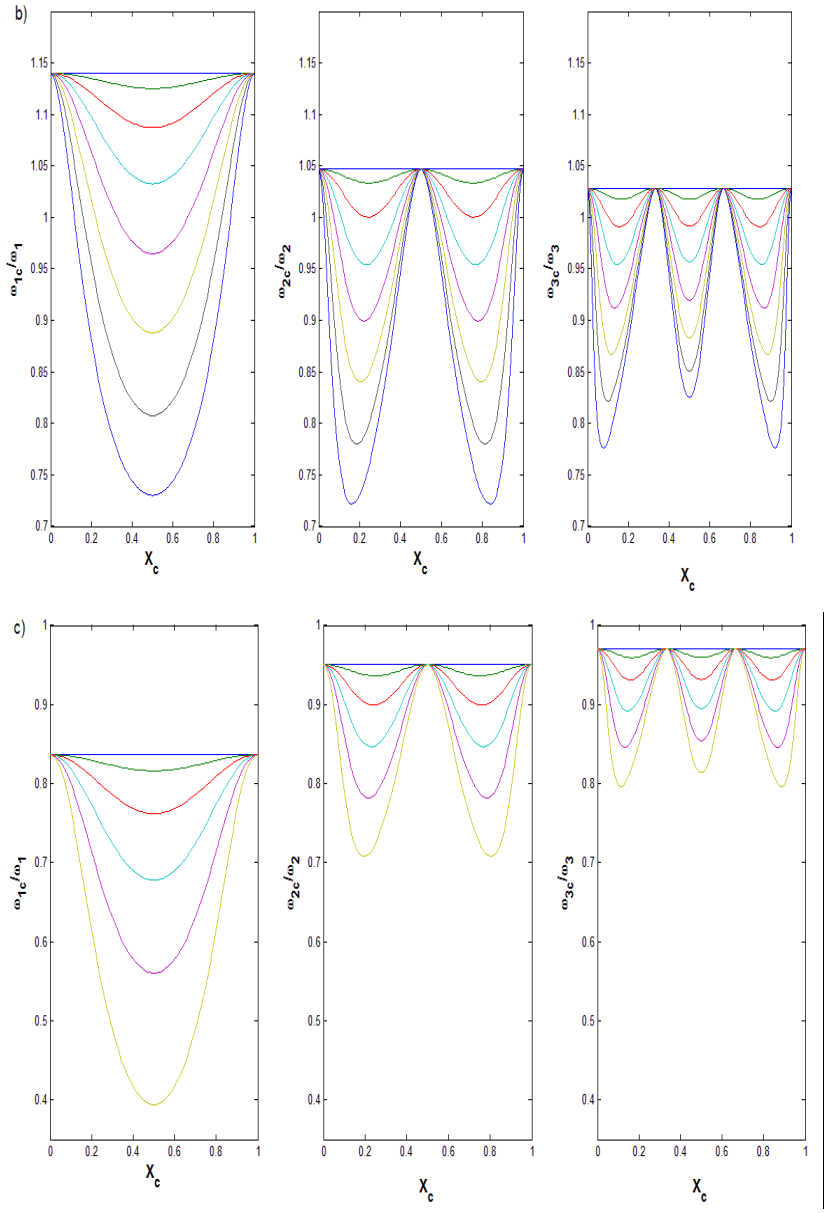

Figure 5. The first three non-dimensional natural frequencies of a hinged-hinged beam with a single crack for a) P/P_{cr}=0, b) P/P_{cr}=–0.3, and c) P/P_{cr}=0.3. The curves are obtained for a/h values of 0, 0.1, 0.2, 0.3, 0.4, 0.5, 0.6, and 0.7 (from top to bottom), and c) P/P_{cr}=0.3 with values of a/h= 0, 0.1, 0.2, 0.3, 0.4, and 0.5.

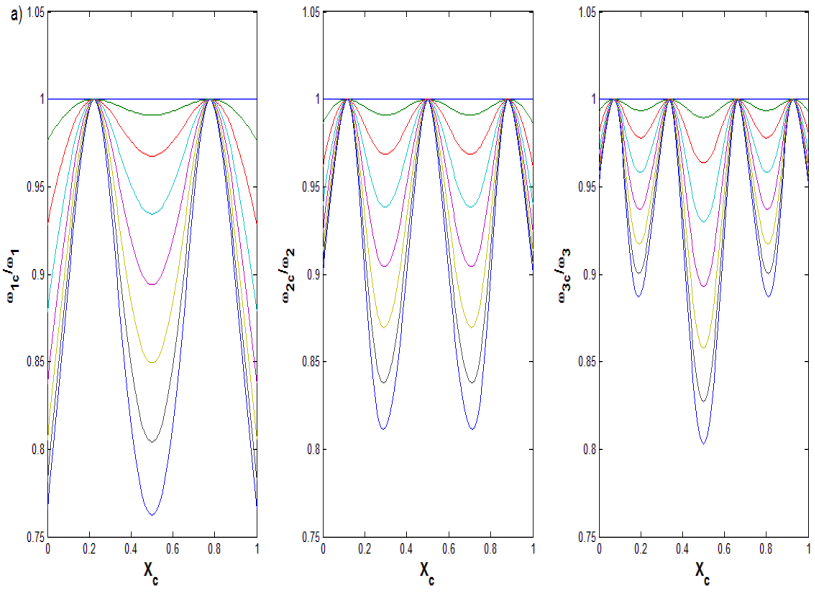

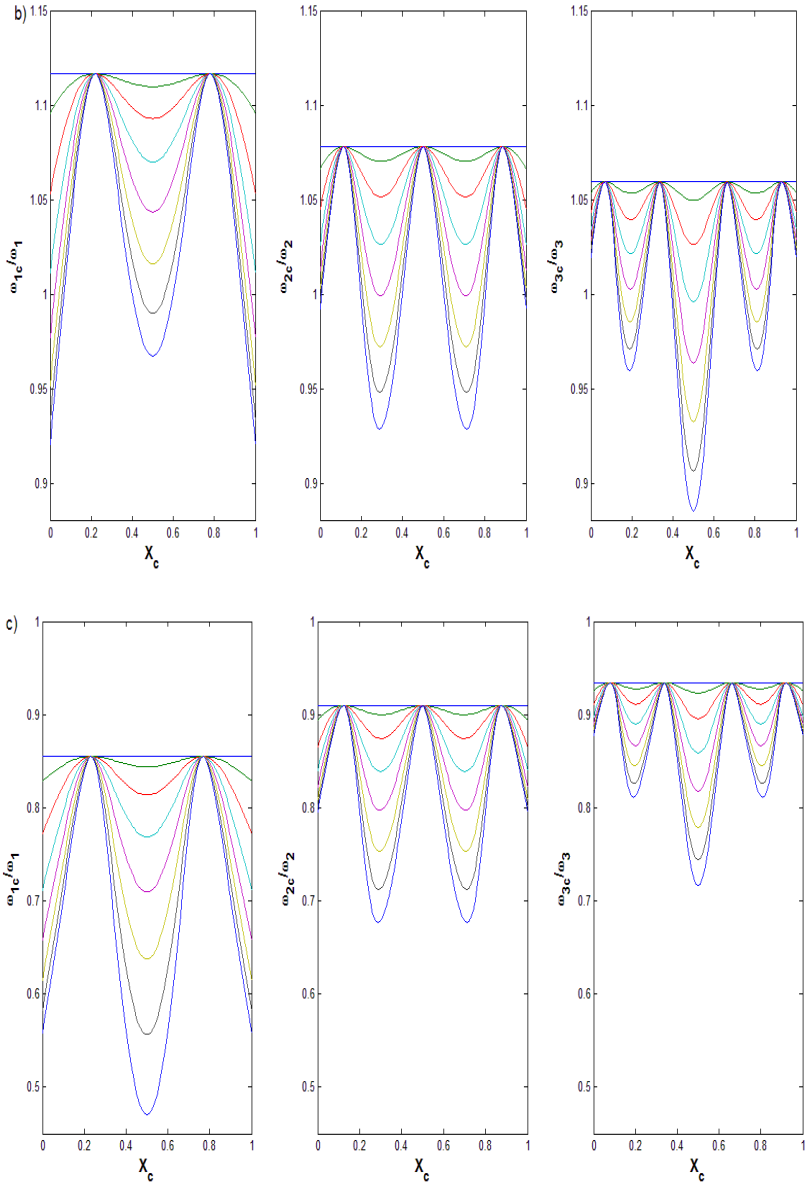

Figure 6. Same as Fig. 5 but with fixed-fixed boundary and values of a/h = 0, 0.1, 0.2, 0.3, 0.4, 0.5, 0.6 and 0.7 for c).

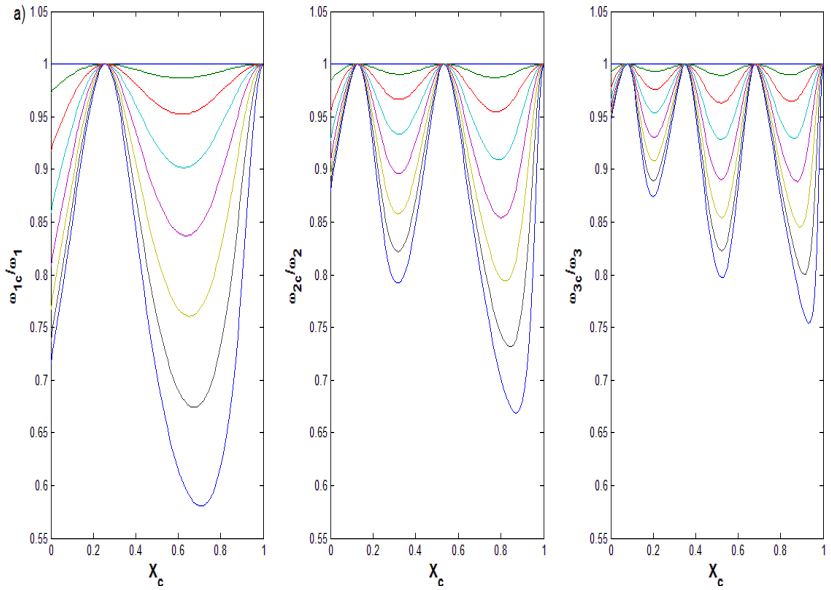

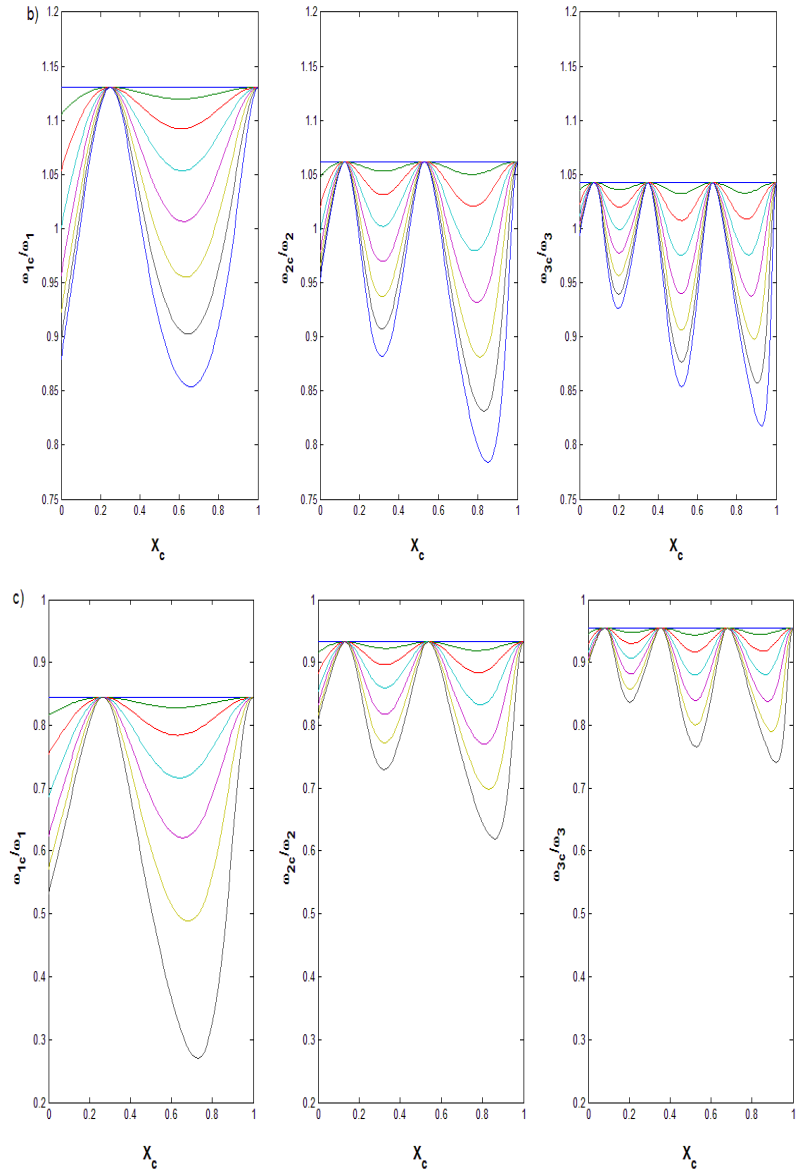

Figure 7. Same as Fig. 5 but with fixed-hinged boundary and values of a/h = 0, 0.1, 0.2, 0.3, 0.4, 0.5, and 0.6 for c).

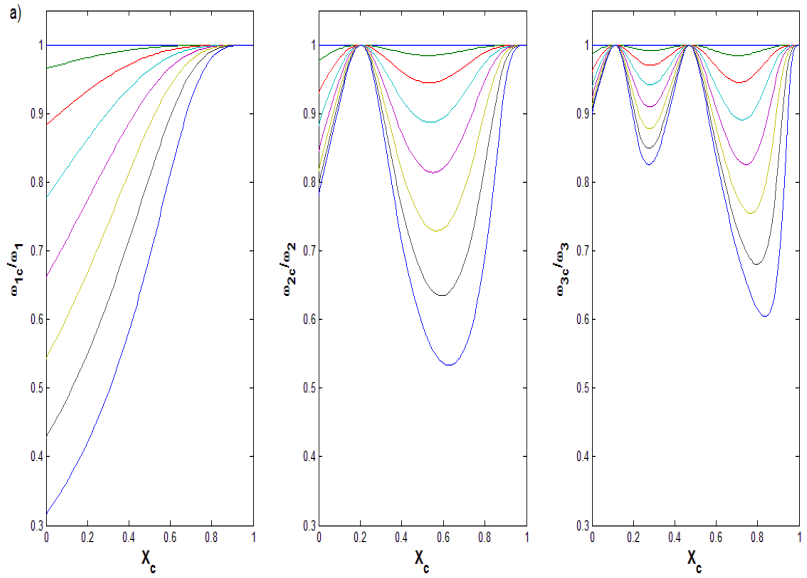

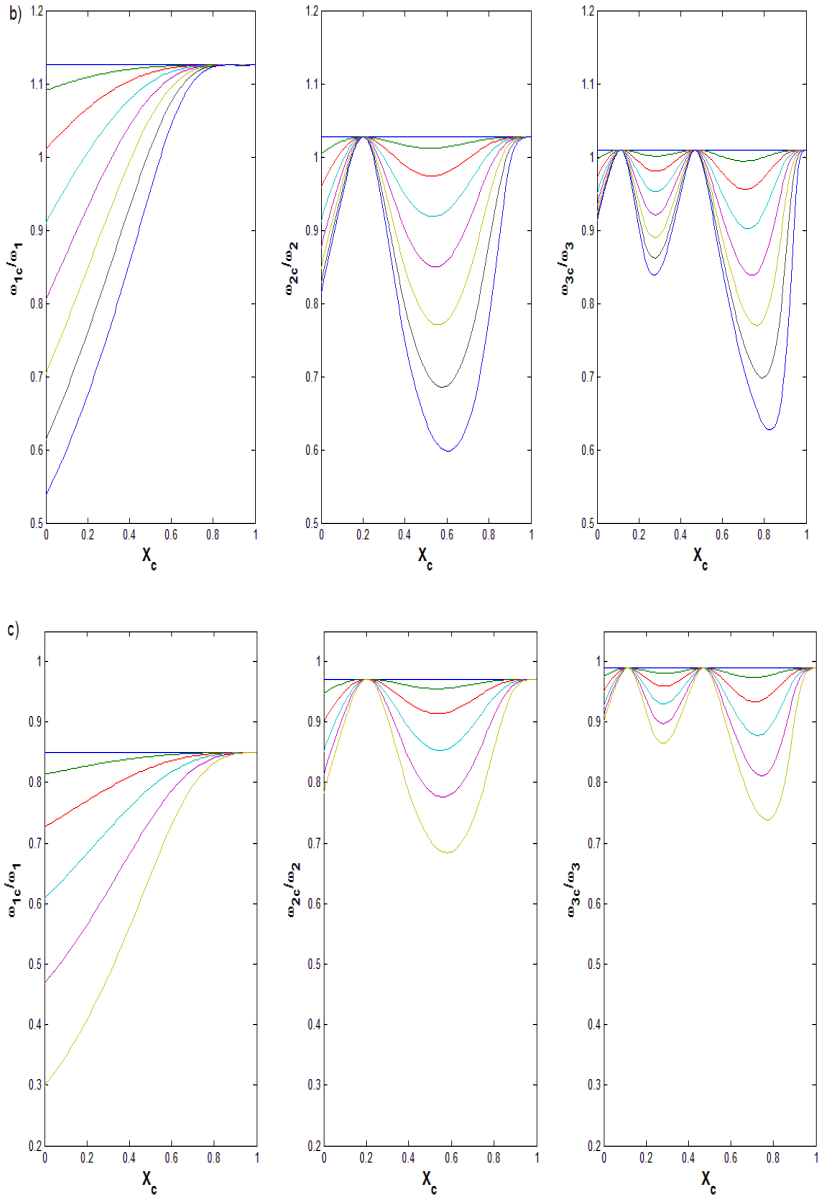

Figure 8. Same as Fig. 5 but with fixed-free boundary and values of a/h = 0, 0.1, 0.2, 0.3, 0.4, and 0.5 for c).

3.3. Effects of multiple cracks and axial load on natural frequencies

Fig. 9 and 10 show the first three non-dimensional natural frequencies of a beam with four cracks versus crack location, for hinged-hinged and fixed-free boundaries, respectively. For brevity, the fixed-fixed and fixed-hinged results are not shown here. Five values of aspect ratio a/h are used in all figures (0, 0.1, 0.2, 0.3, and 0.4). Three cracks are fixed at locations of maximum variation of non-dimensional frequencies: 0.15*l*, 0.5*l*, and 0.85*l*, and at 0.01*l*, 0.6*l*, and 0.8*l* for hinged-hinged and fixed-free boundaries, respectively, while the fourth crack moves along the beam. As seen, the presence of four cracks in the beam lowers the non-dimensional natural frequencies, with or without axial load relative to the case of a single crack. A maximum 17 % and 15 % decrease of the first non-dimensional frequencies is observed for an aspect ratio of 0.4 when the fourth crack is located closer to the supports and mid-span of the beam, for hinged-hinged boundary conditions-compare Fig. 5a) with Fig. 9a). For fixed-free beam, a maximum 14 % and 34 % decrease of the first non-dimensional frequency is observed for an aspect ratio of 0.4 when the fourth crack is closer to the fixed and free supports, respectively-compare Fig. 8 a) with Fig. 10 a). It can be concluded here that the strongest and weakest beam in terms of fundamental natural frequencies is fixed-fixed and fixed-free beam, respectively.

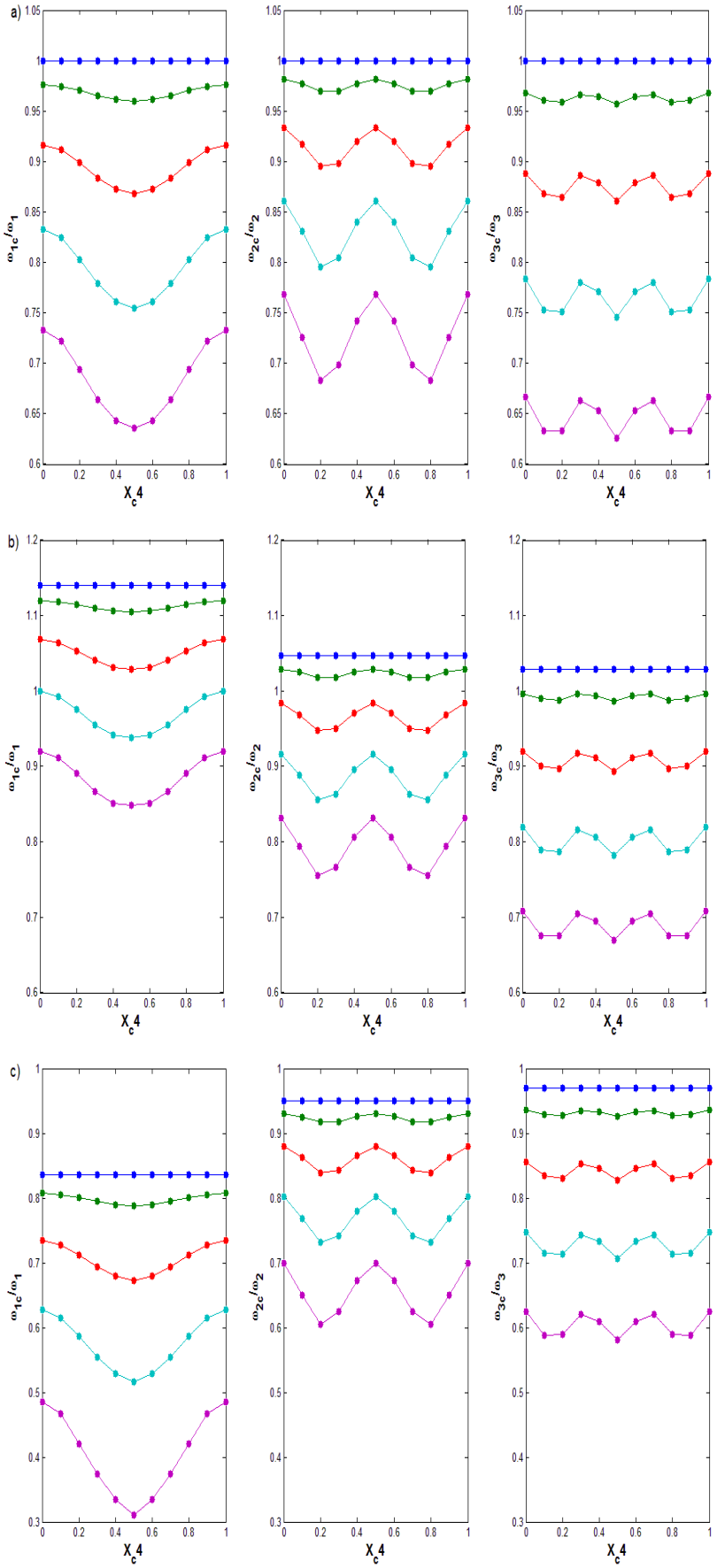

Figure 9. The first three non-dimensional natural frequencies of a hinged-hinged beam with four cracks for a) P/P_{cr}=0, b) P/P_{cr}=–0.3, and c) P/P_{cr}=0.3. The curves are obtained for a/h values of 0, 0.1, 0.2, 0.3, and 0.4 (from top to bottom).

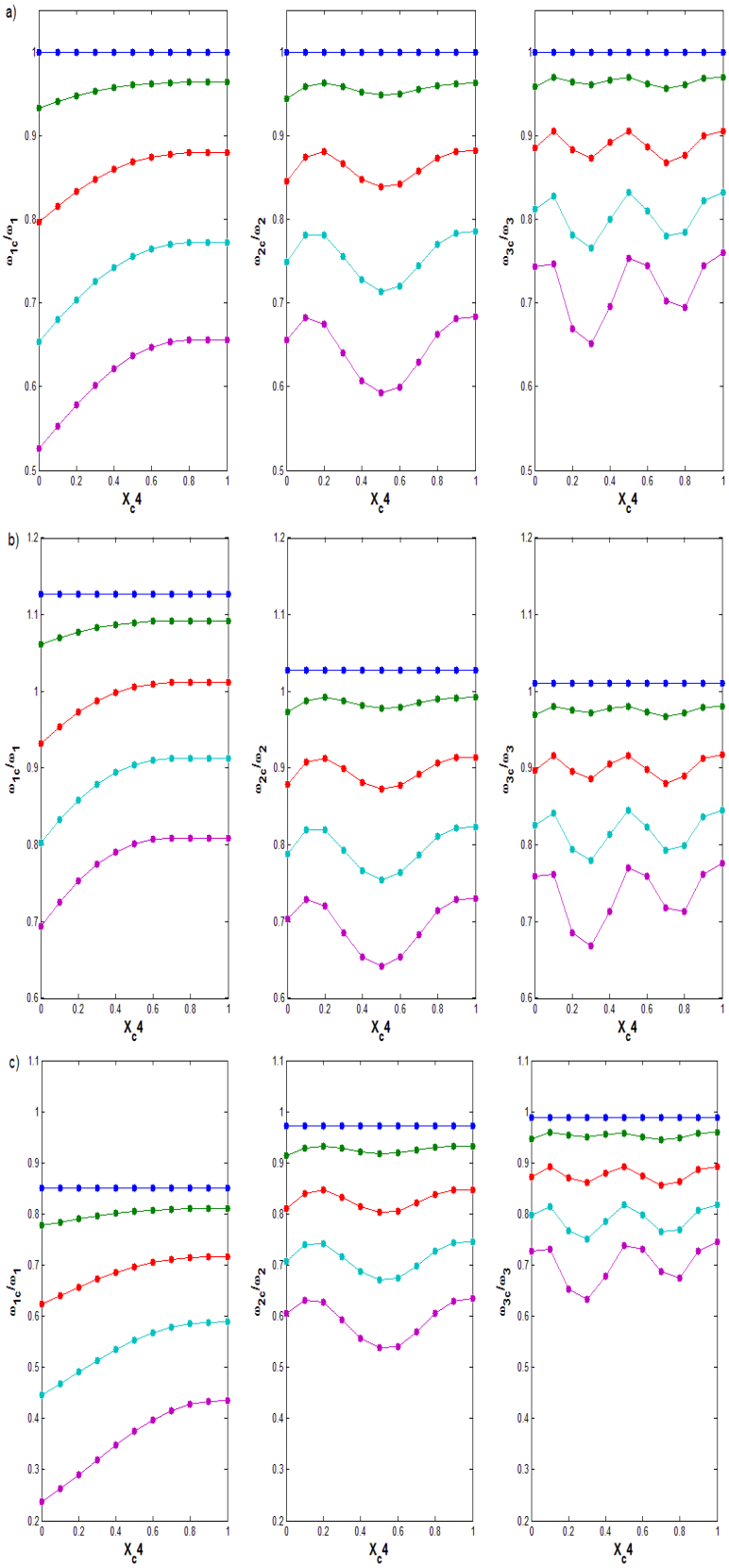

Figure 10. Same as Fig. 9 but with fixed-free boundary.

3.4. Effects of number of cracks on natural frequencies and corresponding mode shapes.

Fig. 11 and 12 show the effect of number of cracks on the first three non-dimensional natural frequencies of a beam for fixed-fixed, and fixed-hinged boundaries, respectively. Again, for brevity, the results of hinged-hinged and fixed-free are not shown here. In all figures, a/h = 0.3 is used, figure a) represents P/P_{cr} = 0, figure b) represents P/P_{cr} = -0.3, and figure c) represents P/P_{cr} = 0.3, the solid line represents a beam with one moving crack, the dashed line represents a beam with two cracks: one crack at location 0.2*l* and one moving

crack along the beam, and the dotted line represents a beam with three cracks, cracks located at 0.2*l* and 0.4*l* and one moving crack along the beam. Increasing the number of cracks leads to a decrease in the non-dimensional natural frequency for all loading cases. Fig. 13 and 14 show the effects of the number of cracks on the first three mode shapes of a beam with hinged-hinged and fixed-free boundaries, respectively. The results of fixed-fixed and fixed-hinged are not shown. Again, in all figures, a/h = 0.3 is used, figure a) represents P/P_{cr} = 0, figure b) represents P/P_{cr} = -0.3, and figure c) represents P/P_{cr} = 0.3. It is clear that the number of cracks slightly affects the mode shapes.

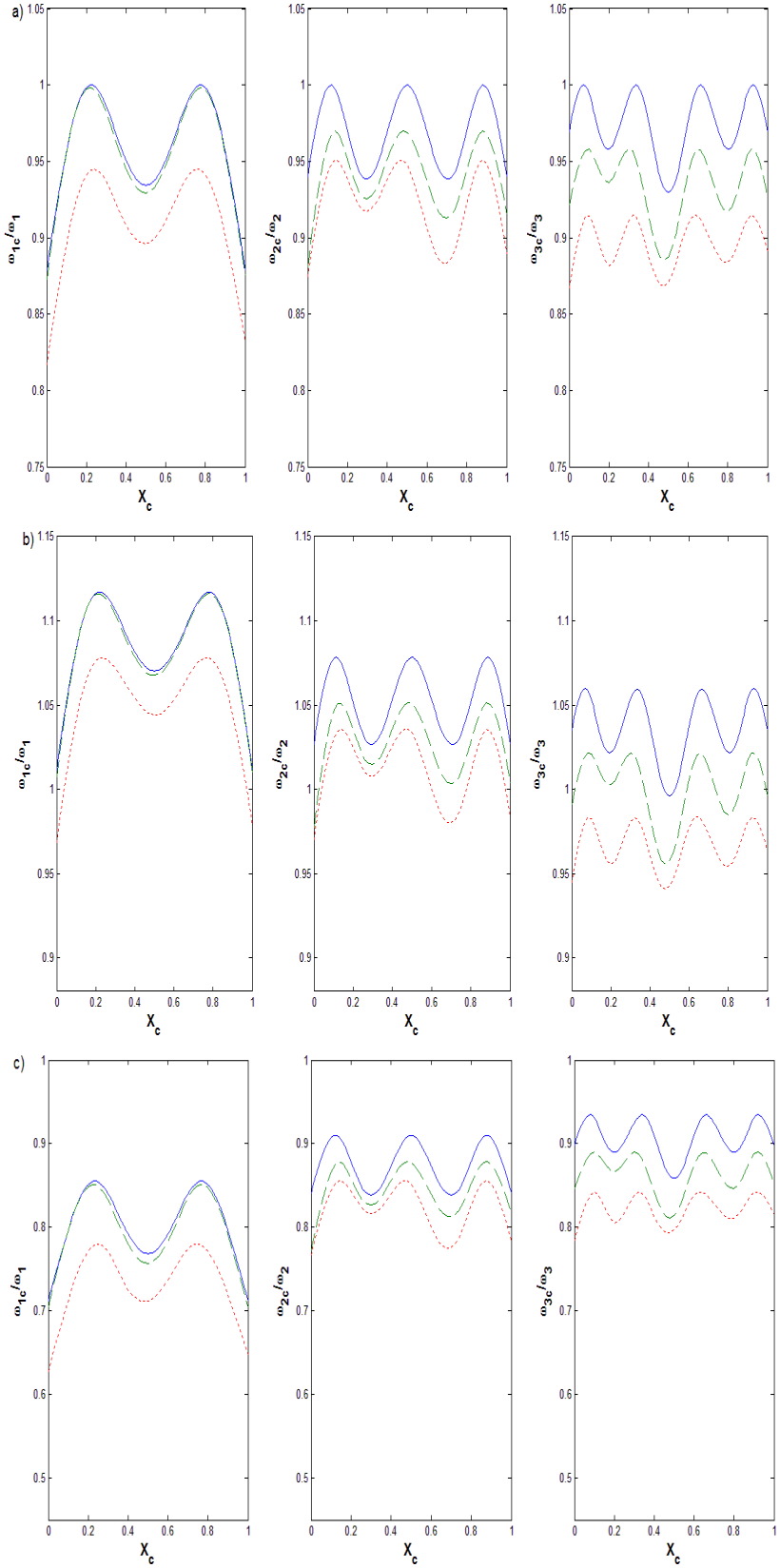

Figure 11. Effects of number of cracks on the first three non-dimensional natural frequencies of fixed-fixed beam for a) *P/P*$_{cr}$=0, b) *P/P*$_{cr}$=–0.3, and c) *P/P*$_{cr}$=0.3.

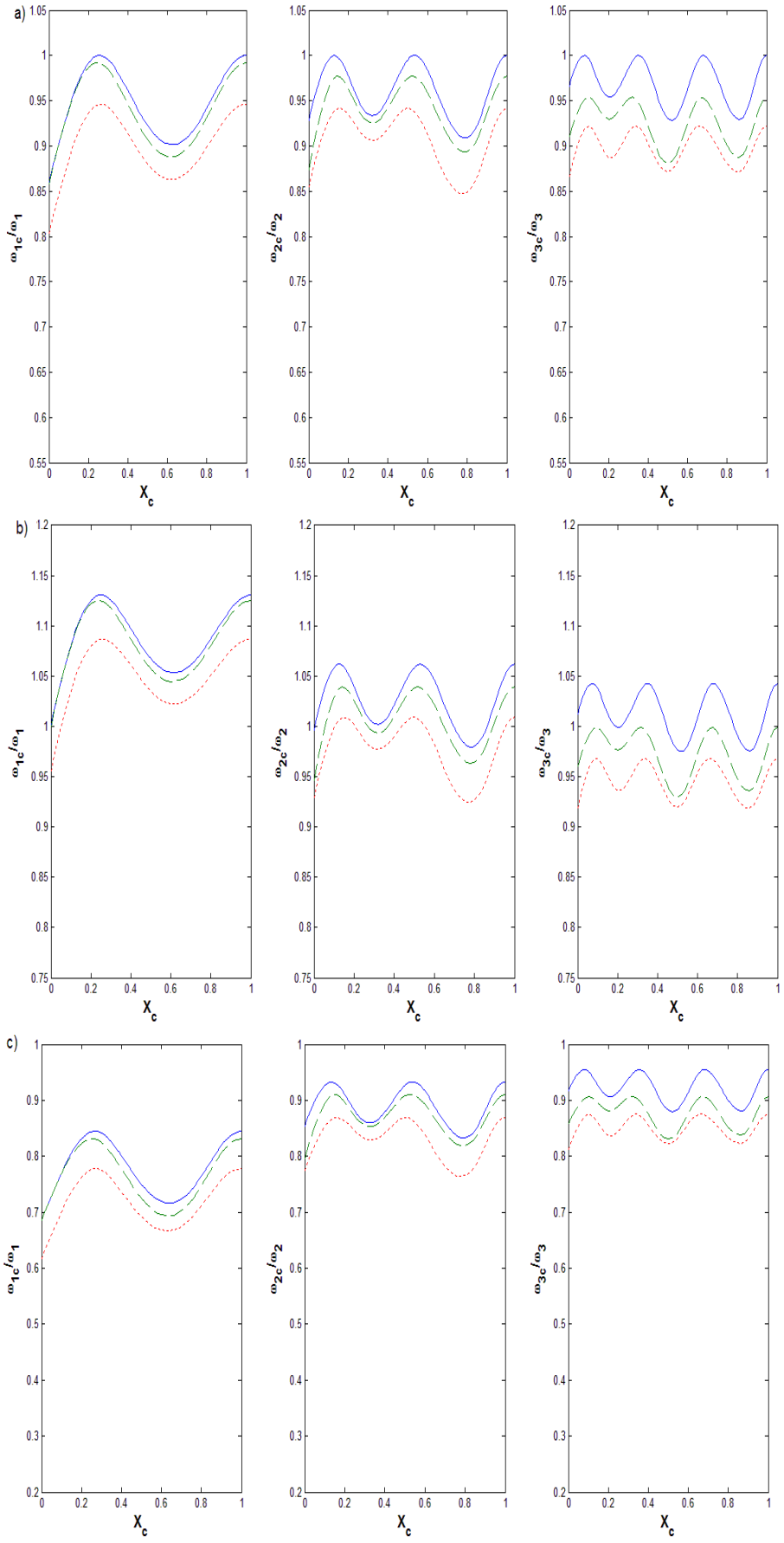

Figure 12. Same as Fig. 11 but with fixed-hinged boundary.

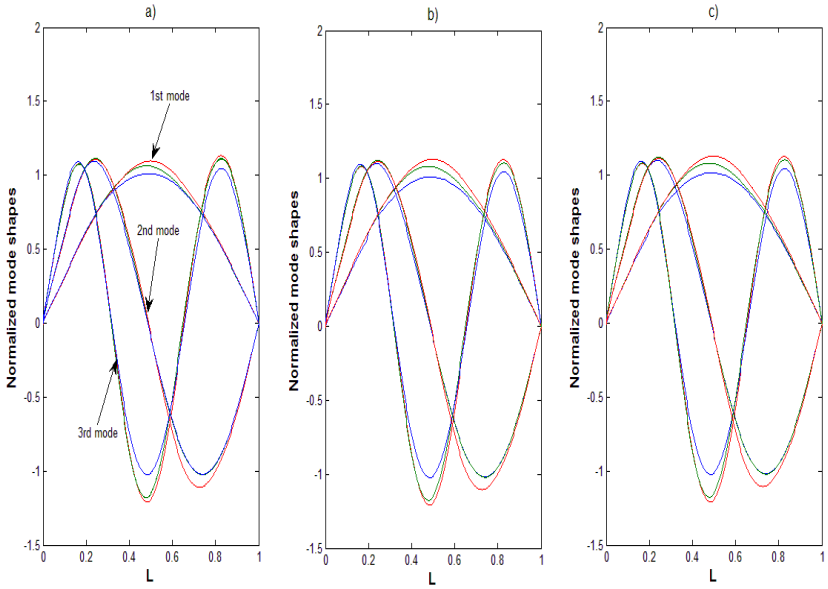

Figure 13. Effects of number of cracks on the first three mode shapes of hinged-hinged beam for a) P/Pcr=0, b) P/Pcr=–0.3, and c) P/Pcr=0.3. (Blue line represents one crack, green line represents two cracks, and red line represents three cracks)

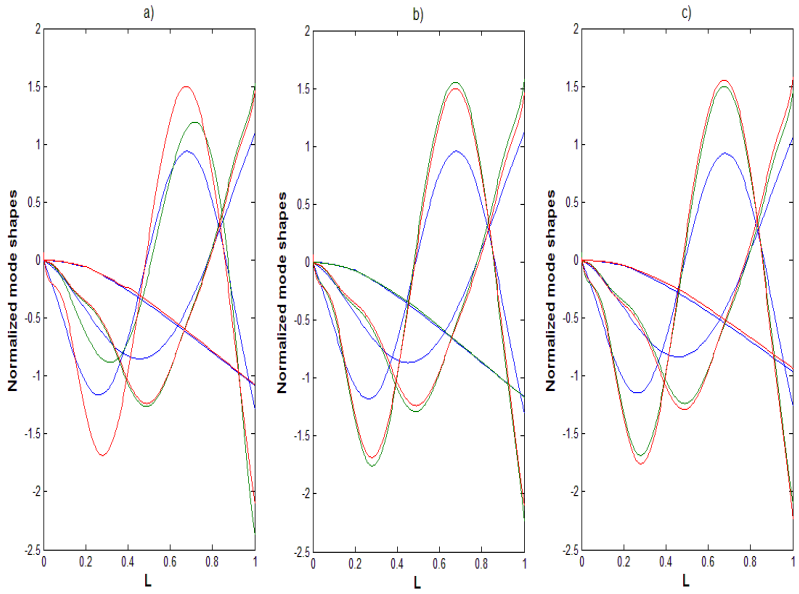

Figure 14. Same as Fig. 13 but with fixed-free boundary.

3.5. Effects of shear deformation and rotational inertia on natural frequencies

Fig. 15 and 16 show the effects of shear deformation and rotational inertia on the first three non-dimensional natural frequencies for fixed-fixed and fixed-hinged boundary conditions, respectively. The results of hinged-hinged and fixed-free are not shown. The y-axis is $\Omega_i = \omega_{ic}\sqrt{\rho / E}$ of the cracked beam and the x-axis is the position of the crack. In all figures, figure a) represents P/P_{cr} = 0, figure b) represents P/P_{cr} = -0.3, and figure c) represents P/P_{cr} = 0.3. Three values of slenderness ratio are used 5, 10, and 20. The value of a/h used is 0.3. It can be seen that the non-dimensional natural frequencies decrease as the value of slenderness increases. Also, it can be seen that the fundamental non-dimensional natural frequencies obtained by EBT and TBT gradually coincide at L/h greater than 10. A remarkable difference is observed on the fundamental non-dimensional natural frequencies obtained by EBT and TBT at L/h less than 10. At higher modes, the effects of L/h become more noticeable for all boundary conditions. In all figures, the results of L/h = 20 are not shown because the EBT and TBT results coincide with each other.

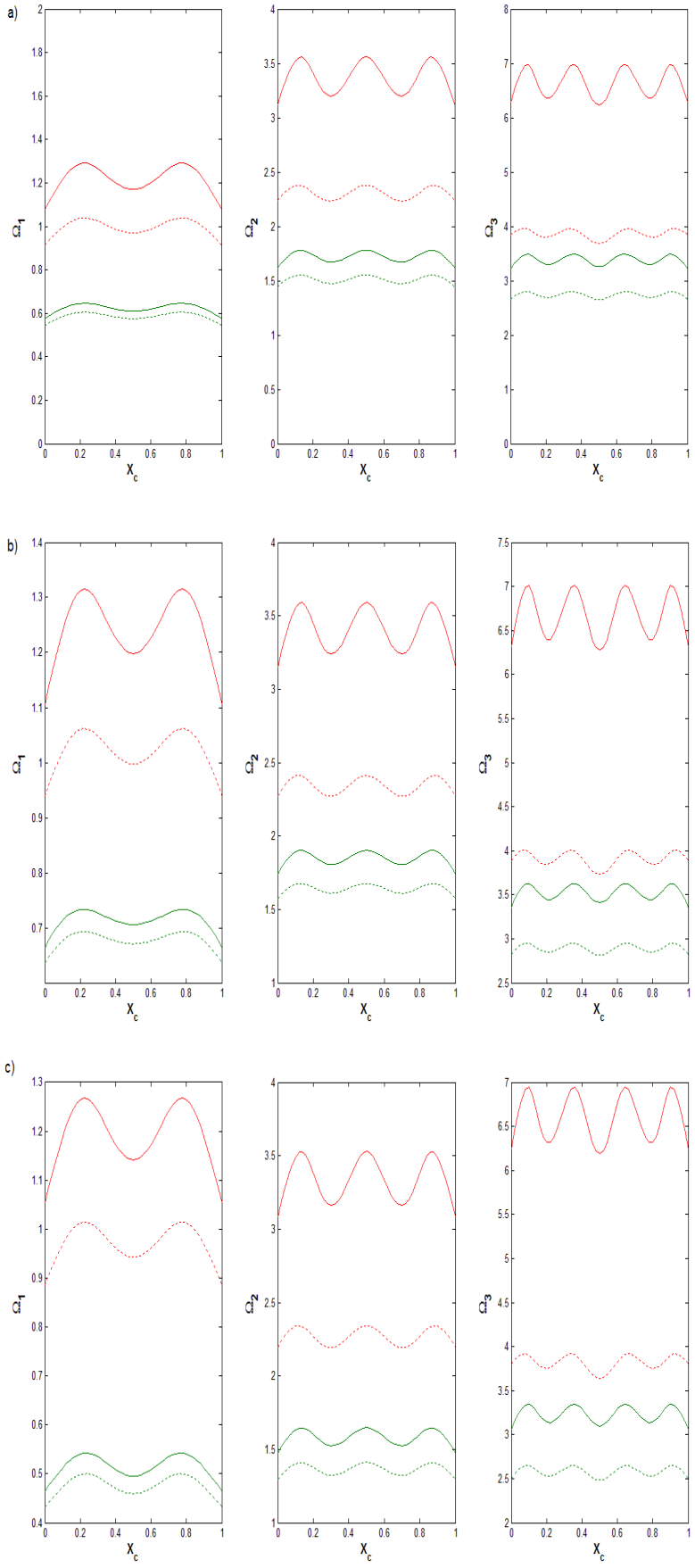

Figure 15. The first three non-dimensional frequencies of fixed-fixed beam with a single crack obtained by Euler– Bernoulli model with L/h = 5, Timoshenko model with L/h = 5, Euler–Bernoulli model with L/h = 10, and Timoshenko model with L/h = 10 (represented by solid red, dashed red, solid green, and dashed green lines, respectively); a) P/P_{cr}=0, b) P/P_{cr}=–0.3, and c) P/P_{cr}=0.3.

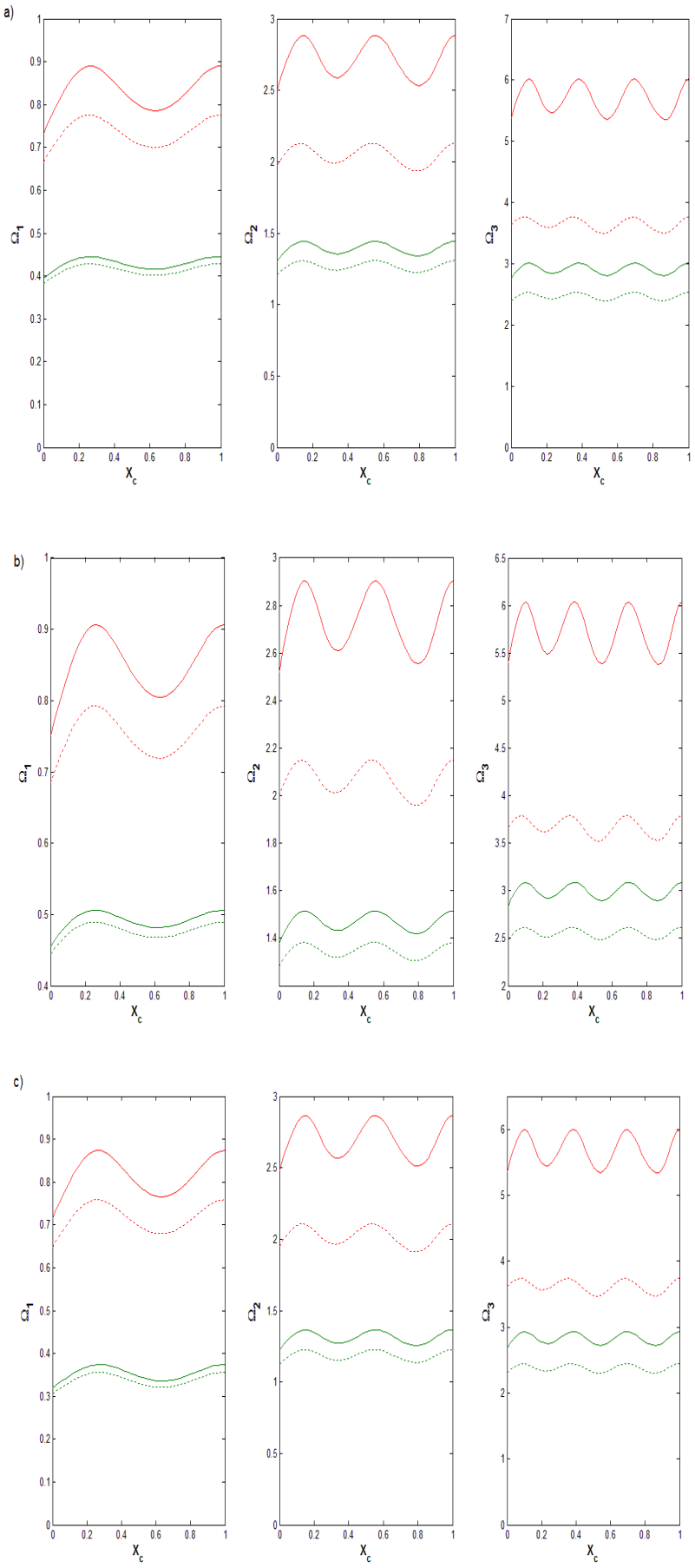

Figure 16. Same as Fig. 15 but with fixed-hinged boundary.

4. Conclusions

A simple transfer matrix method is used to study the vibrational behavior of axially-loaded, multi-cracked Timoshenko beams with differing boundary conditions. The effects of slenderness ratio, axial load, aspect ratio, a/h, boundary conditions, and number of cracks on the non-dimensional natural frequencies and the corresponding mode shapes are investigated. The following conclusions can be drawn:

1. The tensile force stiffens the beam while the compressive force softens the beam.
2. For the first mode, the severity of the cracks and the magnitude of the axial load affect the non-dimensional frequencies.
3. A decrease in the natural frequency is observed as the number of cracks increases, due to increased flexibility of the beam.
4. For specific crack location, the natural frequency decreases as the aspect ratio, a/h, increases.
5. At the location of the zero-crossing of the mode shape, and at critical points along the beam, the natural frequencies do not change with differing aspect ratios.
6. For the first non-dimensional frequencies, the compressive force shifts the locations of critical points toward the center of the beam. The tensile force shifts them toward the supports for fixed-fixed and fixed-hinged boundaries.
7. The first non-dimensional natural frequency is not affected by the crack location, aspect ratio of the crack, or the value of axial load beyond a certain location of the fixed-free beam.
8. A remarkable difference of the non-dimensional natural frequencies obtained by the Euler-Beam theory and Timoshenko beam theory is observed at values of L/h less than 20.

References

1. Liebowitz, H., Claus, W.D. Failure of notched columns, J. Eng. Fract. Mech. 1986. 1. Pp. 379–383. DOI: 10.1016/0013-7944(68)90010-6
2. Dimarogonas, A.D. Vibration of cracked structures: a state of the art review. Engineering Fracture Mechanics, 1996. 55 (5). Pp. 831–857. DOI: 10.1016/0013-7944(94)00175-8
3. Zheng, T., Ji, T. Equivalent representations of beams with periodically variable cross-sections. Engineering Structures. 2011. 33 (3). Pp. 706–719. DOI: 10.1016/j.engstruct.2010.11.007
4. Christides, S., Barr, A.D.S. Torsional vibration of cracked beams of non-circular cross-section. International Journal of Mechanical Sciences. 1986. 28 (7). Pp. 473–490. DOI: 10.1016/0020-7403(86)90067-6
5. Chondros, T.G., Dimarogonas, A. D., Yao, J. A continuous cracked beam vibration theory. Journal of Sound and Vibration. 1998. 215(1). Pp. 17–34. DOI: 10.1006/jsvi.1998.1640
6. Dimarogonas, A.D. Vibration Engineering. West Publishing Company, St. Paul, 1976. 568 p.
7. Liebowitz, H. Vanderveldt, H., Harris, D.W. Carrying capacity of notched columns. International Journal of Solids and Structures. 1967. 3(4). Pp. 489–500. DOI: 10.1016/0020-7683(67)90003-0
8. Liebowitz, H., Claus Jr., W.D. Failure of notched columns. Engineering Fracture Mechanics. 1968. 1(2). Pp. 379–383. DOI: 10.1016/0013-7944(68)90010-6
9. Okamura, H., Liu, H.W., Chu, C.S., Liebowitz, H. A cracked column under compression. Engineering Fracture Mechanics. 1969. 1(3). Pp. 547–564. DOI: 10.1016/0013-7944(69)90011-3
10. Brown, W.F., Srawley, J.E. Plane Strain Crack Toughness Testing of High Strength Metallic Materials. ASTM International. 1966. Pp. 1–129. DOI: 10.1520/STP44663S
11. Tada, H., Paris, P.C., Irwin, G.R. The stress analysis of cracks handbook, 3rd edn. ASME Press, New York .2000. 698 p. DOI: 10.1115/1.801535
12. Fernandez-saez, J., Navarro, C. Fundamental frequency of cracked beams in bending vibrations: an analytical approach. Journal of Sound and Vibration. 2002. 256(1). Pp. 17–31. DOI: 10.1006/jsvi.2001.4197
13. Yoon, H., Son, I., Ahn, S. Free vibration analysis of Euler-Bernoulli beam with double cracks. Journal of Mechanical Science and Technology. 2007. 21(3). Pp. 476–485. DOI: 10.1007/BF02916309
14. Loya, J.A., Rubio, L., Fernandez-saez, J. Natural frequencies for bending vibrations of Timoshenko cracked beams. Journal of Sound and Vibration. 2006. 290(3–5). Pp. 640–653. DOI: 10.1016/j.jsv.2005.04.005
15. Zhong, S.C., Oyadiji, S.O. Analytical predictions of natural frequencies of cracked simply supported beams with a stationary moving mass. Journal of Sound and Vibration. 2008. 311(1–2). Pp. 328–352. DOI: 10.1016/j.jsv.2007.09.009
16. Naguleswaran, S. Vibration and stability of an Euler–Bernoulli beam with up to three-step changes in cross-section and in axial force. International Journal Mechanical Sciences. 2003. 45(9). Pp. 1563–1579. DOI: 10.1016/j.ijmecsci.2003.09.001
17. Gomes, H.M., de Almeida, F.J.F. An analytical dynamic model for single-cracked beams including bending, axial stiffness, rotational inertia, shear deformation and coupling effects. Applied Mathematical Modelling. 2014. 38(3). Pp. 938–948. DOI: 10.1016/j.apm.2013.07.019
18. Aydin, K. Vibratory characteristics of Euler-Bernoulli beams with an arbitrary number of cracks subjected to axial load. Journal of Vibration and Control. 2008. 14(4). Pp. 485–510. DOI: 10.1177/1077546307080028
19. Neves, A.C., Simões, F.M.F., da Costa, A.P. Vibrations of cracked beams: Discrete mass and stiffness models. Computers and Structures. 2016. 168. Pp. 68–77. DOI: 10.1016/j.compstruc.2016.02.007

20. Kwanghun, K., Sok, K.,Kyongjin, S., Pak, C., Kwangbok, H. A modeling method for vibration analysis of cracked beam with arbitrary boundary condition. Journal of Ocean Engineering and Science. 2018. 3(4). Pp. 367–381. DOI: 10.1016/j.joes.2018.11.003
21. Batihan, A.Ç., Kadioğlu, F.S. Vibration Analysis of a Cracked Beam on an Elastic Foundation. International Journal of Structural Stability and Dynamics. 2016. 16(05). 1550006 p. DOI: 10.1142/S0219455415500066
22. Khorram, A., Rezaeian, M., Bakhtiari-Nejad, F. Multiple cracks detection in a beam subjected to a moving load using wavelet analysis combined with factorial design. European Journal of Mechanics A/solids. 2013. 40. Pp. 97–113. DOI: 10.1016/j.euromechsol.2012.12.012
23. Heydari, M., Ebrahimi, A., Behzad, M. Forced vibration analysis of a Timoshenko cracked beam using a continuous model for the crack. Engineering Science and Technology, an International Journal. 2014. 17(4). Pp. 194–204. DOI: 10.1016/j.jestch.2014.05.003
24. Yang, J., Chen. Y., Xiang, Y., Jia, X.L. Free and forced vibration of cracked inhomogeneous beams under an axial force and a moving load. Journal of Sound and Vibration. 2008. 312(1-2). Pp. 166–181. DOI: 10.1016/j.jsv.2007.10.034
25. Khiem, N.T., Lien, T.V., Ninh, V.T.A. Natural Frequencies of Multistep Functionally Graded Beam with Cracks. Iranian Journal of Science and Technology, Transactions of Mechanical Engineering. 2019. 43, Pp. 881–916. DOI: 10.1007/s40997-018-0201-x
26. Lien, T.V., Duc, N.T., Khiem, N.T. Free Vibration Analysis of Multiple Cracked Functionally Graded Timoshenko Beams. Latin American Journal of Solids and Structures. 2017. 14(9). Pp. 1752–1766. DOI: 10.1590/1679-78253693
27. Kou, K.P., Yang, Y. A meshfree boundary-domain integral equation method for free vibration analysis of the functionally graded beams with open edged cracks. Composites Part B: Engineering. 2019. 156. Pp. 303–309. DOI: 10.1016/j.compositesb.2018.08.089
28. Khiem, N.T., Tran, H.T., Nam. D. Modal analysis of cracked continuous Timoshenko beam made of functionally graded material. Mechanics Based Design of Structures and Machines. 2019. DOI: 10.1080/15397734.2019.1639518
29. Chen, W., Chang, H. Vibration Analysis of Functionally Graded Timoshenko Beams. International Journal of Structural Stability and Dynamics. 2018. 18(01). 1850007 p. DOI: 10.1142/S0219455418500074
30. Lien, T.V., Duc, N.T., Khiem, N.T. Free and forced vibration analysis of multiple cracked FGM multi span continuous beams using dynamic stiffness method. Latin American Journal of Solids and Structures. 2019. 16(2). Pp. 1–26. DOI: 10.1590/1679-78255242
31. Chen, B., Zhao, X., Li, Y.H., Guo, Y. Forced vibration analysis of multi-cracked Timoshenko beam with the inclusion of damping by virtue of Green's functions. Applied Acoustics. 2019. 155. Pp. 477–491. DOI: 10.1016/j.apacoust.2019.06.016
32. Khiem, N.T., Huyen, N.N., Long, N.T. Vibration of Cracked Timoshenko Beam Made of Functionally Graded Material. In: Harvie J., Baqersad J. (eds) Shock & Vibration, Aircraft/Aerospace, Energy Harvesting, Acoustics & Optics. Conference Proceedings of the Society for Experimental Mechanics Series. Springer, Cham. 2017. 9. Pp. 133–143. DOI: 10.1007/978-3-319-54735-0_15
33. Lien, T.V., Duc, N.T., Khiem, N.T. Mode Shape Analysis of Multiple Cracked Functionally Graded Timoshenko Beams. Latin American Journal of Solids and Structures. 2017. 14(7). Pp. 1327–1344. DOI: 10.1590/1679-78253496
34. Chouiyakh, H. Azrar, L. Alnefaie, K., Akourri, O. Vibration and multi-crack identification of Timoshenko beams under moving mass using the differential quadrature method. International Journal of Mechanical Sciences. 2017. 120. Pp. 1–11. DOI: 10.1016/j.ijmecsci.2016.11.014
35. Khiem, N.T., Huyen, N.N. A method for crack identification in functionally graded Timoshenko beam. Nondestructive Testing and Evaluation . 2017. 32. Pp. 319–341. DOI: 10.1080/10589759.2016.1226304
36. Pestel, E.C., Leckie, F.A. Matrix methods in elasto mechanics, McGraw-Hill, London, 1963. 435 p.
37. Attar, M. A transfer matrix method for free vibration analysis and crack identification of stepped beams with multiple edge cracks and different boundary conditions. International Journal of Mechanical Sciences. 2012. 57(1). Pp. 19–33. DOI: 10.1016/j.ijmecsci.2012.01.010
38. Khiem, N.T., Lien, T.V. The dynamic stiffness matrix method in forced vibration analysis of multiple-cracked beam. Journal of Sound and Vibration. 2002. 254(3). Pp. 541–555. DOI: 10.1006/jsvi.2001.4109
39. Khiem, N.T., Lien, T.V. A simplified method for natural frequency analysis of a multiple cracked beam. Journal of Sound and Vibration. 2001 245(4). Pp. 737–751. DOI: 10.1006/jsvi.2001.3585
40. Bozyigit, B., Bozyigit, I., Yesilce, Y., Abdel Wahab, M. Crack Identification in Multi-Span Beams on Elastic Foundation by Using Transfer Matrix Method, 2020. Proceedings of the 13th International Conference on Damage Assessment of Structures. Lecture Notes in Mechanical Engineering. Springer, Singapore.
41. Tan, G., Liu, Y., Gong, Y., Shen, Y., Liu, Z. Free Vibration of the Cracked Non-uniform Beam with Cross Section Varying as Polynomial Functions. KSCE Journal of Civil Engineering. 2018. 22(1). Pp. 4530–4546. DOI: 10.1007/s12205-018-1833-5
42. Kisa, M. Vibration and stability of multi-cracked beams under compressive axial loading. International Journal of Physical Sciences. 2011. 6(11). Pp. 2681–2696. DOI: 10.5897/IJPS11.493
43. Nguyen, K.V. Mode shapes analysis of a cracked beam and its application for crack detection. Journal of Sound and Vibration. 2014. 333(3). Pp. 848–872. DOI: 10.1016 /j.jsv.2013.10.006
44. Zheng, D. Y., Kessissoglou, N.J. Free vibration analysis of a cracked beam by finite element method. Journal of Sound and Vibration. 2004. 273(3). Pp. 457–475. DOI: 10.1016 /S0022-460X(03)00504-2
45. Aydin, K. Vibratory characteristics of axially loaded Timoshenko beams with arbitrary number of cracks. Journal of Vibration and Acoustics. 2007. 129(3). Pp. 341–354. DOI: 10.1115/1.2731411
46. Weaver Jr.W., Timoshenko, S.P., Young, D.H. Timoshenko, S., Jr, W.W. Vibration Problems in Engineering. 5th edn. Wiley. New York, 1990. 624 p.
47. Cheng, F.Y. Matrix Analysis of Structural Dynamics: Applications and Earthquake Engineering. 1st edn. Marcel Dekker Inc., New York, 2000. 997 p.
48. Al Rjoub, Y.S., Hamad, A.G. Free Vibration of Axially Loaded Multi-Cracked Beams Using the Transfer 49. Matrix Method. International Journal of Acoustics and Vibration. 2019. 24(1). Pp. 119–138. DOI: 10.20855/ijav.2019.24.11274

Contacts:

Yousef Al Rjoub, ysalrjoub@just.edu.jo

Azhar Hamad, co.azhar@yahoo.com